JOURNAL OF PETROLOGY | VOLUME 55 | NUMBER 7 | PAGES 1317–1351 | 2014 | doi:10.1093/petrology/egu026

# Polymagmatic Activity at the Monogenetic Mt Gambier Volcanic Complex in the Newer Volcanics Province, SE Australia: New Insights into the Occurrence of Intraplate Volcanic Activity in Australia

**J. VAN OTTERLOO[1]*, M. RAVEGGI[1], R. A. F. CAS[1] AND R. MAAS[2]**

[1]SCHOOL OF GEOSCIENCES, MONASH UNIVERSITY, CLAYTON CAMPUS BLD. 28, WELLINGTON ROAD, CLAYTON, VIC. 3800, AUSTRALIA

[2]SCHOOL OF EARTH SCIENCES, UNIVERSITY OF MELBOURNE, MCCOY BUILDING, CARLTON, VIC. 3053, AUSTRALIA

**RECEIVED AUGUST 25, 2013; ACCEPTED APRIL 29, 2014**

*Monogenetic volcanism can produce eruptive suites showing considerable complexity in compositional features and pre-eruptive magma evolution. The ~5 ka Mount Gambier Volcanic Complex (MGVC), a monogenetic volcanic centre in SE Australia's Newer Volcanics Province (NVP), is a good example. It displays a complex stratigraphy of interbedded deposits related to different eruption styles from a multi-vent system. Formation of the MGVC proceeded through simultaneous eruption of two alkali basaltic magma batches: a more alkaline and light rare earth element enriched basanite batch (Mg# 58–62) in the west and a trachybasalt batch (Mg# 58–64) enriched in $SiO_2$ and CaO in the east. Trace element modelling suggests an origin of both magma batches from a single parental melt formed by 4–5% partial melting of a metasomatized lherzolite source in the asthenospheric mantle (2·2 GPa; ~80 km). At the base of the lithosphere, part of this parental melt interacted with a deep-seated pyroxenite contaminant to form the trachybasaltic suite. Further modification of either magma batch at crustal levels appears to have been negligible. Isotope and trace element signatures are consistent with the inferred asthenospheric magma source; Pb isotopes in particular suggest a source with mixed Indian mid-ocean ridge basalt–Enriched Mantle 2 affinities, the latter perhaps related to metasomatic overprinting. It is argued that Cenozoic NVP volcanism in SE Australia is not necessarily related to a mantle plume but can be explained by other models involving asthenospheric upwelling. Fast magma ascent rates in the lithosphere evidenced by the presence of mantle xenoliths may reflect reactivation of lithospheric structures that provide magma pathways to the surface.*

KEY WORDS: *monogenetic volcanism; intraplate basaltic volcanism; southeastern Australia; mantle metasomatism; Gambier Volcanic Complex*

## INTRODUCTION

Monogenetic volcanoes are regarded, in general, as being simple systems of mantle-derived, small-volume, basaltic magmas rising rapidly to the surface (McDonough *et al.*, 1985; Demouchy *et al.*, 2006). They are typically short-lived events, producing single lava shields, scoria cones, tuff cones, tuff rings and maars as a part of monogenetic volcanic fields or as parasitic centres associated with larger polygenetic systems (Walker, 1993; Valentine & Gregg, 2008; Németh, 2010). However, detailed studies of monogenetic systems have, in many cases, revealed considerable complexity; for example, the occurrence of products related to different eruption styles (Sheard, 1978; Cas *et al.*, 1993;

*Corresponding author. Telephone: +61 3 9905 4382. Fax: +61 3 9905 4903. E-mail: jozua.vanotterloo@monash.edu

Strong & Wolff, 2003; Valentine *et al.*, 2007; Clarke *et al.*, 2009; Genareau *et al.*, 2010; Cas & Van Otterloo, 2011; McGee *et al.*, 2012), evolving magma compositions (Blondes *et al.*, 2008; Smith *et al.*, 2008; Ma *et al.*, 2011; McGee *et al.*, 2012), and/or mixing of magmas from different sources (Baker *et al.*, 1997; Reiners, 2002; Németh *et al.*, 2003; Haase & Renno, 2008; Ma *et al.*, 2011; McGee *et al.*, 2013). In some monogenetic centres, multiple magma batches are involved in one or more eruptive events, for which the term 'polymagmatic monogenetic volcanism' has been suggested (Brenna *et al.*, 2010). For example, changes in eruption style at Udo Volcano, South Korea, were caused by changes in magma composition: explosive eruption of alkali basalts was followed by effusive eruption of sub-alkaline compositions (Brenna *et al.*, 2010). In contrast, monogenetic volcanism at Lathrop Wells Volcano, Southwest Nevada Volcanic Field, USA, is characterized by a wide variety of eruption styles, but without major compositional variations (Valentine *et al.*, 2007), whereas compositionally distinct magma batches at Rangitoto Volcano, New Zealand, produced similar volcanic facies (Needham *et al.*, 2011).

Despite their apparent complexity, the monogenetic centres mentioned above are still relatively simple systems in terms of volcanic facies and number and spacing of eruption vents. By contrast, the ~5 ka Mount Gambier Volcanic Complex (Mt. Gambier, MGVC), within the intraplate Newer Volcanics Province (NVP) of southeastern Australia (Fig. 1), is a monogenetic basaltic volcanic centre with a complex stratigraphy, comprising a variety of facies formed by different alternating eruption styles from at least 14 eruption vents aligned along a 3 km long parallel dyke system (Sheard, 1978; van Otterloo *et al.*, 2013). Earlier studies of Mt. Gambier (Irving, 1974; Irving & Green, 1976; Nicholls & Joyce, 1989; Foden *et al.*, 2002; Demidjuk *et al.*, 2007), undertaken largely in the general context of NVP petrogenesis, involved relatively limited sampling, focusing on the eastern lava flows. Based on Sr–Nd isotope data for the well-studied eastern basalt (0·70334–0·70415, $\varepsilon_{Nd}$ +2·5 to +3·2), the MGVC magmas were thought to represent plume-related melts or mixtures derived from the interaction of upwelling asthenosphere with incompatible element-rich lithospheric mantle (McDonough & McCulloch, 1987; Foden *et al.*, 2002; Demidjuk *et al.*, 2007). The Nd isotope data have been used to propose a Neoproterozoic to Cambrian age (0·52–0·64 Ga) for the formation of the underlying lithospheric mantle (Foden *et al.*, 2002). U–Th isotopic disequilibria for the MGVC and the nearby Mt. Schank Volcanic Complex were used to propose an upwelling rate of 1·5 cm $a^{-1}$ in a dynamic melting environment, assuming the model of edge-driven convection (Demidjuk *et al.*, 2007).

In this study we present new major and trace element and Sr–Nd–Pb isotope data based on comprehensive sampling of the recently established detailed stratigraphy of the MGVC (van Otterloo *et al.*, 2013). In contrast to previous studies, which focused on the eastern basalt flow, we included in our study the wide range of deposits dispersed over the entire volcanic complex as well as mantle xenoliths and shallow crustal material. The data show that the deposits were formed by the eruption of two magma batches. From the stratigraphic relationships it is clear that these erupted at the same time, making the MGVC a unique monogenetic centre. This paper examines the petrogenetic evolution of the MGVC basalts with the aim to improve understanding of the petrogenetic complexities of monogenetic volcanic systems. The results are discussed within the context of the Pliocene–Recent intraplate volcanism in SE Australia and are used to comment on the nature of monogenetic volcanic systems.

## REGIONAL GEOLOGY

### The Newer Volcanics Province (NVP) of southeastern Australia

Intraplate basaltic volcanic activity has occurred along Australia's eastern seaboard since the break-up of Gondwana at ~90 Ma (Johnson, 1989). The most recent, Neogene phase of volcanic activity in southeastern Australia (5 Ma–Recent; McDougall *et al.*, 1966; Aziz-ur-Rahman & McDougall, 1972; McDougall & Gill, 1975; Gray & McDougall, 2009) is marked by the development of the intraplate basaltic Newer Volcanics Province, extending ~400 km from Melbourne, Victoria, in the east to Mount Gambier, South Australia, in the west (Fig. 1a). The basement to the NVP basalts comprises Cretaceous–Tertiary sediments of the Otway Basin in the south and Palaeozoic rocks of the Delamerian and Lachlan Orogens in the north (Birch, 2003). The province covers an area of ~25 000 $km^2$ (van Otterloo, 2012) with >400 known eruption centres (Joyce, 1975; Boyce, 2013); however, the total volume of volcanic material is relatively small (1300 $km^3$; Wellman, 1974; Nicholls & Joyce, 1989). Based on geomorphological characteristics, three sub-provinces are recognized (Joyce, 1975): Central Highlands, Western Plains and Mt. Gambier. Although the youngest volcanism occurs at Mt. Gambier, no consistent age trends have been recognized within and between these sub-provinces.

The NVP (particularly the Western Plains sub-province) has been the topic of several geochemical and petrological studies (Irving & Green, 1976; McDonough *et al.*, 1985; Ewart *et al.*, 1988; Johnson, 1989; Whitehead, 1991; Price *et al.*, 1997; Vogel & Keays, 1997; McBride *et al.*, 2001; Foden *et al.*, 2002; Hare *et al.*, 2005). The lithologies range from primitive (Mg# 73–74) nephelinites and picrobasalts (Foden *et al.*, 2002), both occurring only in the Mt. Gambier sub-province, to basanites, sodic and potassic trachybasalts, alkali basalts and more evolved tholeiites, basaltic trachyandesites and phonotephrites scattered across

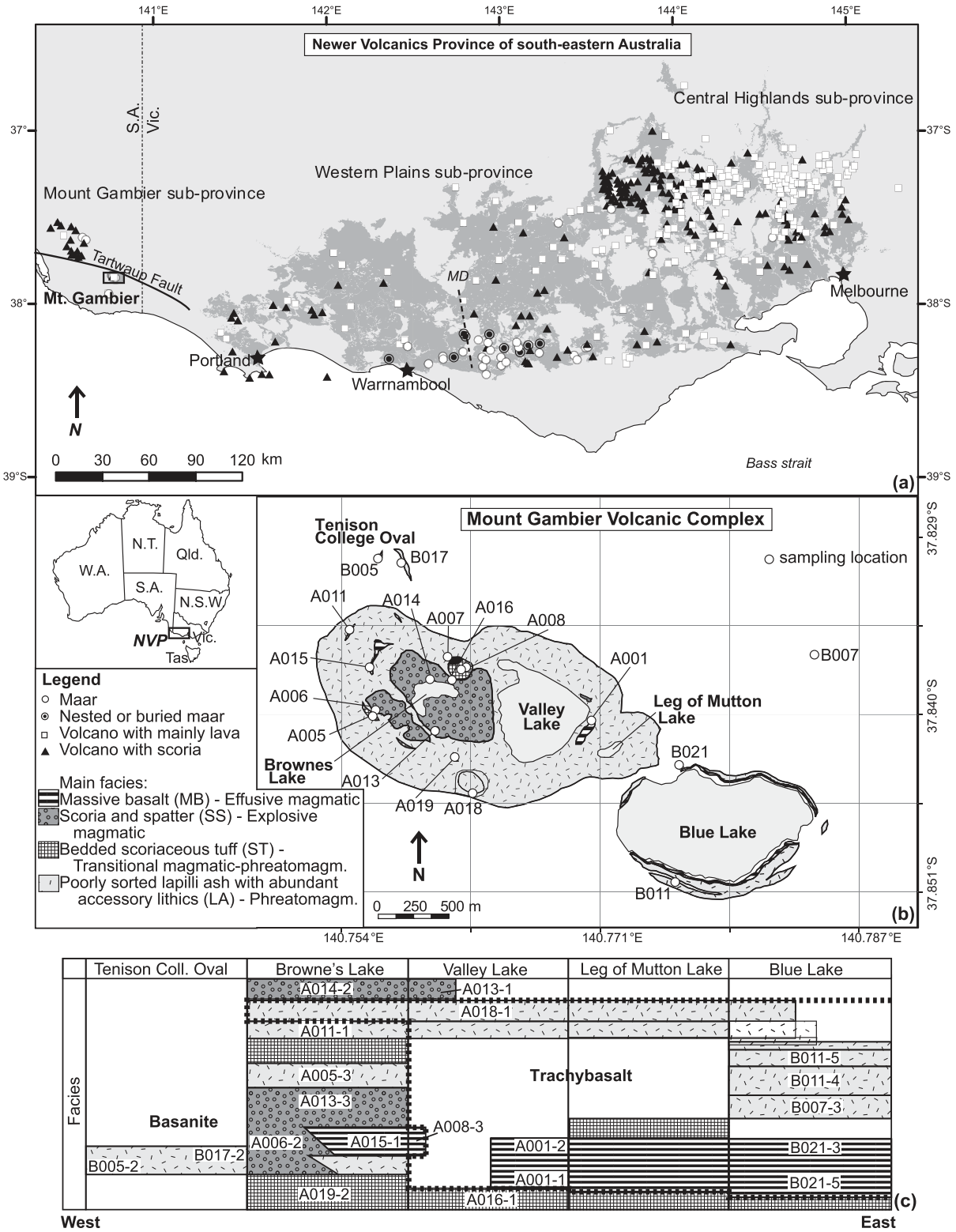


**Fig. 1.** (a) Map of the Newer Volcanics Province of southeastern Australia and its eruption centres (after Joyce, 1975); the Mount Gambier Volcanic Complex (MGVC) is located in its far west. MD, Mortlake Discontinuity, after Price *et al.* (1997). (b) Map of the Mount Gambier Volcanic Complex showing the distribution of the four main facies. Numbers mark the sample locations. (c) Schematic representation of the stratigraphy of the volcanic facies as they have been recorded in the craters and crater walls. Numbers correspond to the analysed juvenile volcanic samples; the first letter and following three digits correspond to the sample locations. The bold dotted line marks the divide between the basanitic suite in the west and the trachybasaltic suite in the east.

the entire province. Basaltic andesite appears to be confined to the Portland region in the far west of the Western Plains (van Otterloo, 2012). Although suggested by previous workers (Gray & McDougall, 2009), there is no strong correlation between the composition of the basalts and their age. The oldest known NVP basalts (King's Quarry, 4·5 Ma; McDougall *et al.*, 1966) are alkali basalts (Paul *et al.*, 2005); however, alkaline compositions were erupted alongside sub-alkaline compositions for most of the subsequent history of the province. Only during the last 500 kyr was the magmatism limited to alkaline compositions. However, it should be noted that age data for the NVP, especially in the context of lithology and assigned eruption centre, are limited. Recent advances in high-precision Ar–Ar dating should change this over the coming years (Matchan & Phillips, 2011).

Compositional provinciality has been the focus of several studies. Price *et al.* (1997) and Vogel & Keays (1997) used major element data to distinguish two lava series within the Western Plains sub-province, the alkaline 'cones' series and the mainly sub-alkaline to transitional 'plains' series. Incompatible element contents of both series show similarities to ocean island basalts (OIB). Comprehensive Sr isotope studies identified two isotopic provinces of contrasting $^{87}Sr/^{86}Sr$ (east 0·7047; west 0·7042; Price *et al.*, 1997), separated by the 'Mortlake Discontinuity' (MD, Fig. 1a) which coincides with the location of the Palaeozoic Moyston Fault, an inferred suture between the Adelaide Fold belt (Delamerian Orogen) in the west and the Lachlan Fold belt in the east (Gray & Foster, 2004). Based on Sr–Pb and Re–Os isotope data, McBride *et al.* (2001) concluded that 'plains series' basalts exhibit a record of crustal assimilation whereas no evidence of significant crustal assimilation has been found in the analysed 'cones series' basalts.

Mantle xenoliths are common in the alkaline series basalts of the Western Plains and Mt. Gambier sub-provinces. Spinel lherzolites (± amphibole ± apatite ± phlogopite) are the dominant type, but garnet lherzolites, dunites, pyroxenites and lower crustal granulites are also present. Xenoliths with modal amphibole and apatite are enriched in Ca, Na, Ti, light rare earth elements (LREE) and large ion lithophile elements (LILE), and are interpreted to record interaction with metasomatic, $H_2O$- and $CO_2$-rich fluids (Frey & Green, 1974; Griffin *et al.*, 1988; O'Reilly & Griffin, 1988; Stolz & Davies, 1988; Yaxley *et al.*, 1998). The abundant xenolith suites have been used to model the southeastern Australian geotherm (O'Reilly & Griffin, 1985, 1996).

The origin and tectonic setting of the Cenozoic intraplate basaltic volcanism in southeastern Australia, including the NVP as its youngest expression, has been widely discussed. A hotspot or hotline beneath eastern Australia was suggested based on the geographical distribution and longevity of volcanic activity in the region (Wellman & McDougall, 1974; Wellman, 1983; Sutherland, 1991), and the apparent change in composition from tholeiitic to alkali basaltic and the OIB-type trace element signatures (McDonough *et al.*, 1985; McDonough & McCulloch, 1987). Problems for hotspot and/or hotline models include the east–west trend of the NVP, which is perpendicular to the northward motion of the Australian Plate (Price *et al.*, 2003), and the lack of obvious age progressions.

Price *et al.* (1988, 1997) and Lister & Etheridge (1989) suggested that Cenozoic magmatism in Victoria was produced by interaction of asthenospheric plumes and/or mantle diapirs, related to the post-95 Ma breakup of Australia and Antarctica, with the sub-continental mantle. In this model, the NVP represents a volumetric peak in the long history of extension-related volcanism along the new continental margin. This hypothesis could explain both the apparent lack of systematic geographical trends in the volcanic activity and the margin-parallel extent of the NVP. However, for the last ~10 Myr southeastern Australia has been under NW–SE compression with mainly dextral shear, caused by the convergent plate motions in the SW Pacific (Hillis *et al.*, 1995; Jones *et al.*, 2000; Jensen-Schmidt *et al.*, 2002; Sandiford *et al.*, 2004); extension-related volcanism during this period would be unlikely.

More recently, Finn *et al.* (2005) included the NVP (and the other Cenozoic basaltic monogenetic fields in eastern Australia) within a large 'diffuse alkaline magmatic province' (DAMP) covering much of the SW Pacific. They suggested that this province originated from the interaction of widespread metasomatized lithospheric mantle with lateral and vertical flows of warm Pacific mantle. These mantle flows followed the sudden detachment and sinking of subducted slabs along the former Gondwana margin in the Late Cretaceous. On a more local scale, Demidjuk *et al.* (2007) proposed that the NVP magmatism is related to upwelling induced by local, edge-driven convection of the asthenosphere. Sudden changes in the thickness of the overlying Australian lithosphere might induce such upwelling.

A link between basaltic magmatism and pre-existing lithospheric structures in the Delamerian and Lachlan Orogens and the Otway Basin was suggested by Lesti *et al.* (2008). It was argued that reactivation of such structures in the late Cenozoic compressive setting would induce shearing and localized transtension; this could then trigger small-volume decompression melting in the underlying shallow mantle.

## Mount Gambier Volcanic Complex (MGVC)

The Mount Gambier Volcanic Complex, located in the Mt. Gambier sub-province of the NVP (Fig. 1), is one of the youngest eruption centres of the entire province, with $^{14}C$ ages as young as ~5 ka for burnt roots under the volcanic

ash and ostracods in Blue Lake (Blackburn, 1966; Barbetti & Sheard, 1981; Blackburn *et al.*, 1982; Gouramanis *et al.*, 2010). Older $^{14}C$ ages of ~28 ka for crater lake sediments (Barton & McElhinny, 1980; Leaney *et al.*, 1995) have been dismissed as a result of 'old-carbon' contamination from Oligocene–Miocene Gambier Limestone (Gouramanis *et al.*, 2010). Multiple eruption vents (>14) produced a series of NW–SE-aligned maars, tuff rings, tuff cones, scoria cones and spatter ramparts (van Otterloo *et al.*, 2013). This alignment is parallel to the nearby Tartwaup Fault System, which is a major lithospheric extensional structure in the westernmost part of the Otway Basin (Finlayson *et al.*, 1994), formed during the break-up between Australia and Antarctica around 95 Ma (Veevers, 1986). Tertiary sediments underlying the volcanic deposits reach a thickness of >1 km and comprise sands, shale and limestone (Boult *et al.*, 2002). Accidental lithic fragments of the shallower aquifer-bearing units, limestone and marls of Gambier Limestone (Oligocene–Miocene) and sandstone and clays of the Dilwyn Formation (Middle Eocene), are commonly found in MGVC pyroclastic units.

The volcanic deposits exhibit a wide variety of facies (Sheard, 1978; van Otterloo *et al.*, 2013) related to different eruption styles: effusive magmatic, explosive magmatic (i.e. Hawaiian, micro-Plinian and violent Strombolian), dry and wet phreatomagmatic, and phreato-Vulcanian. In total, six main facies have been recognized based on deposit characteristics, although this number reduces to four if classification is based on petrographic features of the juvenile components alone (Fig. 1b and c; Table 1): massive basalt (MB), scoria and spatter (SS), bedded scoriaceous tuff (ST), and poorly sorted lapilli ash (LA). All facies contain mantle xenoliths (Frey & Green, 1974; McDonough & McCulloch, 1987; Song, 1994; van Otterloo *et al.*, 2013) notably Cr-diopside lherzolites (Group 1 type lherzolites; Frey & Prinz, 1978) but also dunites and pyroxenites; some xenoliths contain amphibole.

Although all the eruption vents are aligned, the volcanic stratigraphy indicates that there is no simple temporal progression of eruption activity along the fissure system. Stratigraphic relations suggest that the oldest and youngest eruption phases both occur in the western part of the complex, and during the entire eruption interval activity occurred in the east and west simultaneously (van Otterloo *et al.*, 2013). Further, no systematic temporal–spatial trends are identified in the production of different facies types. Neither erosional–weathered surfaces nor evidence of soil formation is found between facies, indicating that eruptive events occurred continuously, with only short periods of quiescence (van Otterloo *et al.*, 2013).

The massive basalt facies found around the Blue and Valley Lakes in the east of MGVC (Fig. 1b) has been the main focus of previous studies; it has been classified as *ne*-hawaiite (Irving & Green, 1976). In the western part of the volcanic complex, to the west of Browne's Lake, another massive basalt lava unit crops out, which represents a different flow (Sheard, 1978; van Otterloo *et al.*, 2013). This western basalt unit, as well as pyroclastic units across the complex, have not previously been analysed and classified geochemically.

The eruptive volume and magnitude of the MGVC eruption were determined by van Otterloo & Cas (2013). In total $3{\cdot}25 \times 10^8\,m^3$ of tephra (both juvenile and lithic material) was erupted, equating to $1{\cdot}98 \times 10^8\,m^3$ dense-rock equivalent (DRE) of magmatic material. A minimum volume of $0{\cdot}39 \times 10^8\,m^3$ DRE was estimated for associated magmatic intrusions, giving a minimum volume of magma of $2{\cdot}37 \times 10^8\,m^3$ DRE. With modelled plume heights up to 10 km, the magnitude of the eruption is estimated to be four on the Volcanic Explosivity Index (VEI; Newhall & Self, 1982; van Otterloo & Cas, 2013).

## ANALYTICAL METHODS

Samples for geochemical and isotopic analysis were collected based on our new volcanic stratigraphy model for the MGVC (Fig. 1c; van Otterloo *et al.*, 2013). These include 30 samples of juvenile pyroclastic material and massive basalt from single beds within all main facies in three sectors coincident with the elongated shape of the MGVC: Browne's Lake (west), Valley Lake (centre) and Blue Lake (east). Three lithic fragments representing the main units in the local basement (sandstone, limestone and clay) were collected from a phreatomagmatic volcanic breccia at location A007 (Fig. 1b). Six spinel lherzolite xenolith samples were collected from two sites within the Blue Lake crater walls.

Juvenile pyroclastic lapilli and coarse-ash size (>1 mm) juvenile fragments from the phreatomagmatic and transitional magmatic–phreatomagmatic facies were sieved, handpicked and then cleaned ultrasonically and by scrubbing with a steel brush and a toothbrush. Clean rock chips from both the fragmental and coherent rock samples were milled in a tungsten carbide mill. Because of potential contamination from the mill, the analytical results for Ta and Co are not used here. Milling-related Nb contamination is unlikely to be a problem because the Nb contents of the samples are high (30–100 ppm). The excellent correlation of Nb with Zr confirms that Nb artefacts are absent.

Major element concentrations were determined by X-ray fluorescence (Bruker-AXS S4 Pioneer, operated by Spectra Plus software) at James Cook University using standard techniques. After ignition at 1000°C (4 h), fused discs were prepared using a Li-metaborate–tetraborate flux at 1050–1100°C. Analytical errors for major element results are better than ±1% (1SD). Ferric and ferrous iron are reported together as total $Fe_2O_3$.

*Table 1: The main volcanic facies of the Mount Gambier Volcanic Complex, inferred eruption styles and modal mineralogy of the main phenocrysts*

| Facies | Main facies type | Inferred eruption style | Description | Modes |
|---|---|---|---|---|
| MB | Massive basalt (Facies 1) | Effusive | Pahoehoe and transitional pahoehoe–'a'a lava flows | Massive basalts:<br>Ol 12–17% (west); 3–4% (east)<br>Cpx 1–2% (west); 1–4% (east)<br>Pl 1–2% (west); 2–10% (east)<br>En 1–2%<br>Total phenocrysts: 17% (west); 12% (east)<br>Agglutinates (west only):<br>Ol <22%<br>Cpx 2–8%<br>Pl 5–8%<br>En <5%<br>Total phenocrysts: 34% |
| SS | Scoria and spatter (Facies 2 and 3) | Explosive magmatic | Spatter, agglutinates and scoriae with minor ash | Ol 4–6%<br>Cpx 2–3%<br>Pl 2–3%<br>Total phenocrysts: 19% |
| ST | Bedded scoriaceous tuff (Facies 5 and 6) | Transitional magmatic–phreatomagmatic | Well-bedded scoriae and abundant ash with a small amount of accidental lithic fragments (mainly limestone, minor sandstone) | Ol 10–33%<br>Cpx microlites only<br>Pl microlites only<br>Total phenocrysts: 10–33% |
| LA | Poorly sorted lapilli ash with abundant accessory lithic fragments (Facies 4) | Phreatomagmatic | Bedded to massive, poorly sorted ash and lapilli, and block–lapilli–ash deposits with large amounts of accidental lithic fragments limestone and sandstone) | Ol <30%<br>Cpx <10%<br>Pl <20%<br>Total phenocrysts: <30% |

More detailed descriptions have been given by van Otterloo *et al*. (2013). Facies numbers refer to the facies identified by van Otterloo *et al*. (2013) based on the fragmentation characteristics.

Rare earth and selected trace element analyses were carried out by inductively coupled plasma mass spectrometry (ICP-MS) at the School of Geosciences, Monash University, using a Thermo Finnigan X series II, quadrupole ICP-MS system. Sample solutions were produced from ~50 mg of sample powder. The powders were put into Savillex sealed Teflon vials with a mixture of HF–$HNO_3$–HCl and placed on a hot plate at 150°C for ~48 h. Subsequently the samples were dried down and taken back into solution using 3% $HNO_3$ for final presentation to the mass spectrometer. ICP-MS count rates were externally standardized by means of calibration curves based on the in-house basalt standard BNB. Drift corrections were based on a bi-elemental (indium, bismuth) spike added to each sample solution, and on the variability of standard solutions interspersed with the unknowns. Reproducibility on replicate analyses and accuracy is of the order of 5% for all elements.

Sr–Nd–Pb isotopic data were acquired at the University of Melbourne following methods modified from Maas *et al*. (2005). Whole-rock powders or acid-leached (6 M HCl, 100°C, 60 min) chips were used for Sr–Nd isotope analyses of basalts, and leached chips were used for two mantle xenoliths; all Pb isotope data were acquired on leached chips. Lithic inclusions of sandstone and limestone were analysed after total dissolution at high pressure (HF–$HNO_3$–HCl) and partial dissolution at low pressure (warm nitric acid leach), respectively. Pb, Sr and Nd were

extracted using a combination of anion exchange and EICHROM RE, LN and SR resin chromatography. Blanks were <100 pg and are negligible. Isotopic analyses were carried out on a Nu Plasma multicollector (MC)-ICP-MS system. Sr and Nd isotope ratios were normalized to $^{86}Sr/^{88}Sr = 0{\cdot}1194$ and $^{146}Nd/^{144}Nd = 0{\cdot}7219$, using the exponential law, and are reported relative to SRM987 = 0·710230 and La Jolla Nd = 0·511860. External precision (2SD) is $\leq \pm 0{\cdot}000040$ for $^{87}Sr/^{86}Sr$ and $\pm 0{\cdot}000020$ for $^{143}Nd/^{144}Nd$. Pb mass bias was corrected using thallium doping and a $^{205}Tl/^{203}Tl$ ratio of 2·3871. For signal sizes near 10 V total Pb, this produces internal precisions of $\leq \pm 0{\cdot}01\%$ (2SE) and external precisions of 0·025–0·05% (2SD) in $^{206,207,208}Pb/^{204}Pb$ ratios. The Pb runs for the two spinel lherzolite xenoliths produced smaller signals with higher internal uncertainties; external precision for these samples is expected to be $\sim \pm 0{\cdot}15\%$ (2SD).

USGS basalt and other isotope standards analysed during this study yielded the following results: BCR-2, 0·704995, 0·704978, 0·512636; BHVO-2, 0·703457, 0·703465, 0·512983; JNd-1, 0·512113, 0·512121, 0·512110; EN-1, 0·709151. Five runs of SRM981-Pb yielded the following averages: $^{206}Pb/^{204}Pb$ 16·933 ± 4, $^{207}Pb/^{204}Pb$ 15·483 ± 6, $^{208}Pb/^{204}Pb$ 36·685 ± 16 (all errors 2SD). All results compare well with thermal ionization mass spectrometry and MC-ICP-MS reference values (e.g. Woodhead & Hergt, 1997; Tanaka *et al.*, 2000; Doucelance & Manhès, 2001; Raczek *et al.*, 2003; Baker *et al.*, 2004; Elburg *et al.*, 2005; McArthur *et al.*, 2006; Weis *et al.*, 2006).

# RESULTS

## Petrographic descriptions

All volcanic samples contain phenocrysts in a glassy matrix with varying amounts of microcrysts. Phenocryst phases are mainly olivine, minor augite and rare plagioclase (Fig. 2; Table 1), with variable modal abundances. Phenocrysts occur as single crystals within the groundmass or as glomerocrysts. Coarse olivines include resorbed xenocrysts and newly formed euhedral phenocrysts; the largest of the euhedral olivines (0·50–1·00 mm) contain small glass inclusions (~10–100 μm). Resorbed xenocrystic enstatite is present in some samples.

Mantle xenoliths (spinel lherzolite, dunite, typically 1–5 cm, although some are up to 15 cm in diameter) are present in the fragmental facies types (i.e. SS, LA and ST), and smaller xenoliths (~0·5 cm) are occasionally found in the coherent facies (MB). Most xenoliths have angular shapes and lack significant resorption or recrystallization at the edges. Their internal texture is mainly equigranular with crystal sizes of ~0·5–1·0 mm (up to 2 mm). Some xenoliths show internal shearing fabrics and foliation; however, there is no relationship between the overall shape of the xenoliths within the basalt and their internal texture, suggesting that the internal texture is a source-inherited characteristic rather than evidence of shearing and plastic behaviour during host magma ascent. This indicates a high ascent rate for the magma carrying these inclusions (>10 cm $s^{-1}$; Spera, 1980).

## Major and trace elements

Major element concentrations and CIPW norms are presented in Table 2. On a total alkali vs silica diagram (Le Bas *et al.*, 1986; Le Maitre *et al.*, 2002) the samples occupy two distinct clusters (Fig. 3a); those from the western MGVC plot in the tephrite–basanite field and those from the eastern MGVC in the trachybasalt field. The trachybasalts can be classified as potassic trachybasalts ($K_2O > Na_2O$). Being more sodic, specimen A001-1 from the eastern massive basalts is an exception: it is from a locality sampled in earlier studies and is best described using the *ne*-hawaiite classification of Irving & Green (1976). All of the potassic trachybasalts from the eastern MGVC, as well as A001-1, are referred to as trachybasalts below. Based on their CIPW norms, the western suite can be classified as basanites (normative olivine >10%) in the basalt tetrahedron (Fig. 3b; Yoder & Tilley, 1962). By comparison, trachybasalts of the eastern MGVC plot near the transition between alkali–olivine basalt and basanite.

The trachybasalts of the eastern MGVC have higher Mg# (57·7·0–63·6 vs 57·8–61·6), $SiO_2$ (46·8–50·6 vs 46·2–47·0 wt %) and CaO (8·5–9·6 vs 8·2–8·6 wt %; a single basanite sample has 9·6 wt %), and lower alkalis and $P_2O_5$ than the basanites of the western MGVC (Fig. 3c–j). $Fe_2O_3t$ increases overall with decreasing Mg# values in the trachybasalts (11·3–12·5 wt %) but not in the western basanites (11·9–12·2 wt %).

As for alkalis and P (Fig. 3), concentrations of LILE and high field strength elements (HFSE) are consistently higher in the basanitic suite (Fig. 4; Table 2). Ni and Cr extend to lower abundances in the basanites compared with the trachybasalts. Based on Mg#, Ni and Cr, the most primitive sample from the western basanites is A015-1 (Mg# 61·6, 165 ppm Ni, 310 ppm Cr), and A001-1 (63·6, 178 ppm, 348 ppm) is the most primitive sample in the trachybasalt dataset. Even more primitive compositions were, however, reported by Irving & Green (1976), Foden *et al.* (2002) and Demidjuk *et al.* (2007).

REE and primitive mantle normalized incompatible element patterns for both magmatic suites (Fig. 5) are strongly fractionated, a characteristic feature in many alkaline series lavas of the Western Plains basalts (Fig. 1a); the REE patterns resemble those typical of OIB (Fig. 5a). The western basanites are more enriched in LREE and incompatible elements than the eastern trachybasalts.

The mantle xenoliths show greater compositional diversity than their basaltic hosts. REE abundances in six analysed spinel lherzolites are low (≤1 × chondrite, Fig. 5c) and extend the field defined by depleted lherzolite xenoliths from other parts of the NVP. Similarly, incompatible

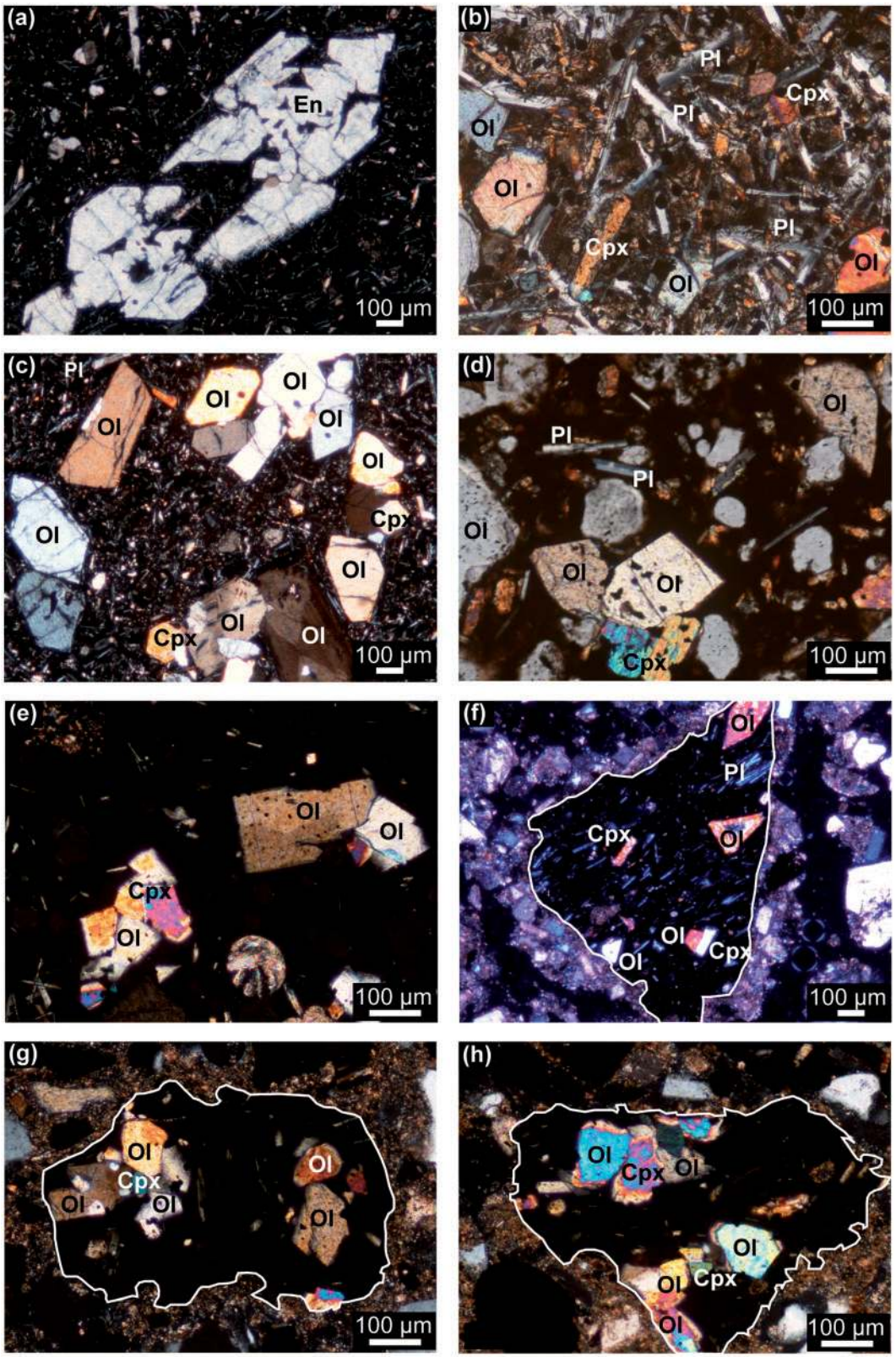


**Fig. 2.** Photomicrographs of the main facies types under cross-polarized light: (a) skeletal enstatite xenocryst; (b) massive basalt facies from the western lava flow unit, MB; (c) eastern lava flow unit, MB; (d) agglutinate, SS; (e) scoria clast, SS; (f) crystalline juvenile clast in ash matrix, LA; (g) glassy juvenile clast in ash, LA; (h) scoria clast in ash matrix, ST.

*Table 2: Major and trace elements and isotope data of representative samples of the basalts from the Mount Gambier Volcanic Complex*

| Lithology: | Basanite | | | | | | | | | | | | |
|---|---|---|---|---|---|---|---|---|---|---|---|---|---|
| Sample: | A005-3 | A006-2 | A008-3 | A011-1 | A013-3 | A014-2 | A015-1 | A016-1 | B005-2 | B016-1 | 963-Ga3 | 963-Ga5 | 963-C |
| $SiO_2$ | 46·22 | 46·70 | 46·72 | 46·61 | 46·23 | 46·64 | 46·57 | 45·86 | 46·44 | 48·13 | 47·25 | 47·2 | 47·25 |
| $TiO_2$ | 2·60 | 2·49 | 2·53 | 2·51 | 2·66 | 2·49 | 2·53 | 2·77 | 2·50 | 2·65 | 2·43 | 2·47 | 2·43 |
| $Al_2O_3$ | 13·41 | 13·48 | 13·58 | 13·57 | 13·74 | 13·44 | 13·40 | 13·92 | 13·50 | 14·34 | 13·55 | 13·55 | 13·55 |
| $Fe_2O_3$ total | 11·69 | 11·89 | 11·92 | 11·82 | 12·03 | 11·96 | 12·08 | 12·12 | 11·94 | 11·37 | 12 | 11·94 | 12 |
| MnO | 0·16 | 0·16 | 0·17 | 0·16 | 0·16 | 0·17 | 0·16 | 0·16 | 0·17 | 0·15 | 0·17 | 0·17 | 0·17 |
| MgO | 7·71 | 8·51 | 8·26 | 8·33 | 7·86 | 8·46 | 8·68 | 7·45 | 8·55 | 5·91 | 8·51 | 8·37 | 8·51 |
| CaO | 9·58 | 8·19 | 8·51 | 8·42 | 8·51 | 8·46 | 8·55 | 8·53 | 8·35 | 9·19 | 8·38 | 8·48 | 8·38 |
| $Na_2O$ | 4·37 | 4·40 | 4·53 | 4·45 | 4·47 | 4·36 | 4·16 | 4·67 | 4·44 | 4·05 | 4·79 | 4·35 | 4·79 |
| $K_2O$ | 2·65 | 2·61 | 2·31 | 2·57 | 2·70 | 2·54 | 2·40 | 2·79 | 2·55 | 2·64 | 2·53 | 2·32 | 2·53 |
| $P_2O_5$ | 0·95 | 0·88 | 0·85 | 0·88 | 0·95 | 0·85 | 0·83 | 1·02 | 0·87 | 0·86 | 0·86 | 0·87 | 0·86 |
| $SO_3$ | 0·04 | 0·05 | b.d. | 0·07 | 0·04 | 0·02 | 0·01 | 0·05 | 0·06 | 0·05 | 0·01 | 0 | b.d. |
| Total | 99·38 | 99·37 | 99·39 | 99·38 | 99·36 | 99·39 | 99·38 | 99·35 | 99·38 | 99·34 | 100·48 | 99·72 | 100·47 |
| Mg# | 59·50 | 61·50 | 60·70 | 61·10 | 59·28 | 61·20 | 61·60 | 57·80 | 61·47 | 53·66 | 61·24 | 60·97 | 61·24 |
| an | 9·43 | 9·64 | 10·07 | 9·87 | 9·68 | 9·81 | 11·00 | 9·07 | 9·75 | 13·52 | 8·76 | *11·56* | 8·76 |
| ab | 11·87 | 16·26 | 17·08 | 15·73 | 14·34 | 15·68 | 16·39 | 13·11 | 15·29 | 20·80 | 17·82 | 20·29 | 17·82 |
| or | 15·90 | 15·66 | 13·89 | 15·42 | 16·25 | 15·25 | 14·42 | 16·78 | 15·31 | 15·84 | 17·56 | *16·12* | 17·56 |
| ne | 13·78 | 11·50 | 11·83 | 11·95 | 12·95 | 11·74 | 10·48 | 14·49 | 12·18 | 7·44 | 15·91 | 12·24 | 15·91 |
| di | 26·37 | 20·87 | 22·02 | 21·61 | 21·77 | 21·98 | 21·51 | 22·01 | 21·47 | 22·10 | 20·54 | 19·01 | 20·54 |
| ol | 11·90 | 15·60 | 14·72 | 14·92 | 14·01 | 15·17 | 15·79 | 13·11 | 15·49 | 9·74 | 12·61 | 13·67 | 12·61 |
| mt | 3·45 | 3·51 | 3·51 | 3·48 | 3·55 | 3·52 | 3·57 | 3·57 | 3·52 | 3·35 | 2·01 | 2·97 | 2·01 |
| il | 5·01 | 4·81 | 4·88 | 4·84 | 5·13 | 4·81 | 4·88 | 5·36 | 4·82 | 5·11 | 2·92 | 2·23 | 2·92 |
| ap | 2·22 | 2·06 | 1·99 | 2·06 | 2·25 | 1·99 | 1·95 | 2·41 | 2·04 | 2·02 | 1·86 | 1·90 | 1·86 |
| hy | 0·00 | 0·00 | 0·00 | 0·00 | 0·00 | 0·00 | 0·00 | 0·00 | 0·00 | 0·00 | 0·00 | 0·00 | 0·00 |
| qz | 0·00 | 0·00 | 0·00 | 0·00 | 0·00 | 0·00 | 0·00 | 0·00 | 0·00 | 0·00 | 0·00 | 0·00 | 0·00 |

| Lithology: | Trachybasalt | | | | | | | | | Limestone | Sandstone | Red clay | Standard |
|---|---|---|---|---|---|---|---|---|---|---|---|---|---|
| Sample: | A001-1 | A001-2 | B007-3 | B011-4 | B011-5 | B021-3 | B021-5 | 963-Ga4 | 2180 | A007-2 | A007-3 | A007-4 | BHVO 1 |
| $SiO_2$ | 46·87 | 47·63 | 50·94 | 50·29 | 68·87 | 47·89 | 46·51 | 49·28 | 48·43 | 12·61 | 75·89 | 51·26 | 45·67 |
| $TiO_2$ | 2·46 | 2·38 | 2·59 | 2·40 | 0·97 | 2·44 | 2·53 | 2·18 | 2·38 | 0·15 | 0·57 | 0·25 | 2·74 |
| $Al_2O_3$ | 13·09 | 13·27 | 12·41 | 11·38 | 6·61 | 14·05 | 13·22 | 13·47 | 13·57 | 2·12 | 2·23 | 5·10 | 14·45 |
| $Fe_2O_3$ total | 12·41 | 12·27 | 11·14 | 14·38 | 5·33 | 12·15 | 12·37 | 12·25 | 11·37 | 0·90 | 5·25 | 28·04 | 12·68 |
| MnO | 0·16 | 0·16 | 0·14 | 0·18 | 0·06 | 0·16 | 0·16 | 0·16 | 0·17 | 0·02 | 0·13 | 0·28 | 0·15 |
| MgO | 9·01 | 8·63 | 7·17 | 8·79 | 3·16 | 8·10 | 8·97 | 9·07 | 8·69 | 19·13 | 4·77 | 1·64 | 7·03 |
| CaO | 9·44 | 9·41 | 9·19 | 6·49 | 12·74 | 8·49 | 9·27 | 8·88 | 9·58 | 63·67 | 10·16 | 11·26 | 7·24 |
| $Na_2O$ | 3·55 | 3·53 | 3·20 | 2·73 | 0·50 | 3·76 | 3·69 | 3·59 | 3·52 | 0·23 | 0·07 | b.d. | 4·23 |
| $K_2O$ | 1·84 | 1·63 | 1·96 | 1·91 | 0·88 | 1·88 | 2·02 | 1·46 | 1·69 | 0·79 | 0·51 | 1·43 | 2·1 |
| $P_2O_5$ | 0·63 | 0·56 | 0·69 | 0·76 | 0·18 | 0·58 | 0·69 | 0·47 | 0·58 | 0·13 | 0·05 | 0·26 | 0·9 |
| $SO_3$ | 0·02 | 0·04 | 0·06 | 0·12 | 0·07 | 0·01 | 0·02 | 0 | b.d. | 0·08 | 0·14 | 0·11 | 0·02 |
| Total | 99·5 | 99·5 | 99·5 | 99·4 | 99·4 | 99·5 | 99·5 | 100·8 | 100 | 99·83 | 99·77 | 99·64 | 98·57 |
| Mg# | 61·80 | 61·03 | 61·90 | 61·80 | 56·96 | 63·92 | 61·76 | 62·26 | 63·00 | 62·26 | 60·24 | 61·14 | 63·00 |
| an | 14·65 | 22·42 | 27·11 | 15·20 | 13·55 | 17·43 | 17·05 | 17·84 | 17·75 | 17·84 | 16·40 | 17·55 | 17·75 |
| ab | 18·73 | 15·92 | 14·07 | 26·29 | 3·86 | 26·46 | 13·83 | 31·28 | 25·66 | 31·28 | 26·16 | 27·48 | 25·66 |
| or | 11·05 | 9·81 | 11·76 | 13·66 | 5·26 | 13·15 | 12·11 | 10·16 | 11·80 | 10·16 | 11·29 | 10·39 | 11·80 |
| ne | 6·28 | 4·12 | 0·00 | 0·00 | 0·00 | 5·64 | 7·88 | 2·08 | 4·78 | 2·08 | 5·71 | 3·99 | 4·78 |
| di | 23·24 | 22·44 | 22·30 | 10·32 | 26·08 | 16·57 | 22·86 | 18·21 | 20·28 | 18·21 | 20·40 | 19·65 | 20·28 |
| ol | 16·12 | 15·70 | 4·06 | 2·46 | 7·13 | 14·24 | 16·09 | 14·72 | 13·48 | 14·72 | 13·66 | 14·65 | 13·48 |
| mt | 3·65 | 3·61 | 3·28 | 2·76 | 1·57 | 2·27 | 3·64 | 2·06 | 2·12 | 2·06 | 2·31 | 2·33 | 2·12 |
| il | 4·75 | 4·60 | 4·99 | 2·96 | 1·86 | 2·94 | 4·86 | 2·63 | 2·87 | 2·63 | 2·84 | 2·77 | 2·87 |
| ap | 1·48 | 1·32 | 1·62 | 1·71 | 0·42 | 1·27 | 1·62 | 1·03 | 1·27 | 1·03 | 1·25 | 1·18 | 1·27 |
| hy | 0·00 | 0·00 | 10·69 | 24·40 | 0·00 | 0·00 | 0·00 | 0·00 | 0·00 | 0·00 | 0·00 | 0·00 | 0·00 |
| qz | 0·00 | 0·00 | 0·00 | 0·00 | 40·17 | 0·00 | 0·00 | 0·00 | 0·00 | 0·00 | 0·00 | 0·00 | 0·00 |

(continued)

*Table 2: Continued*

| Lithology: | Basanite | | | | | | | | | | | | |
|---|---|---|---|---|---|---|---|---|---|---|---|---|---|
| Sample: | A005-3 | A006-2 | A008-3 | A011-1 | A013-3 | A014-2 | A015-1 | A016-1 | B005-2 | B016-1 | 963-Ga3 | 963-Ga5 | 963-C |
| Li | 11·47 | 9·63 | 8·27 | 9·65 | 10·30 | 9·14 | 11·49 | 10·16 | 9·63 | 10·14 | 7·08 | | |
| Be | 2·99 | 3·02 | 2·87 | 3·03 | 3·07 | 2·87 | 2·81 | 3·17 | 2·96 | 3·05 | 2·98 | | |
| Sc | 15·05 | 16·03 | 16·52 | 15·91 | 15·54 | 16·58 | 16·91 | 14·67 | 16·08 | 16·01 | 18·8 | 18·2 | 17 |
| V | 175·51 | 174·46 | 174·88 | 171·11 | 171·73 | 174·07 | 181·48 | 169·74 | 172·64 | 176·92 | 176 | 174 | 163 |
| Cr | 236·20 | 283·75 | 287·79 | 284·14 | 252·78 | 308·01 | 309·98 | 183·46 | 296·50 | 353·43 | 297 | 279 | 258 |
| Mn | 1232·41 | 1281·73 | 1242·89 | 1238·15 | 1266·21 | 1250·23 | 1250·81 | 1283·55 | 1252·30 | 1301·68 | | | |
| Co | 41·49 | 44·65 | 44·06 | 44·19 | 42·32 | 44·41 | 45·53 | 41·74 | 45·19 | 44·86 | 205 | 166 | 161 |
| Ni | 131·31 | 163·44 | 155·54 | 160·38 | 135·58 | 160·14 | 164·77 | 116·62 | 169·59 | 146·72 | 205 | 166 | 161 |
| Cu | 39·13 | 44·00 | 45·94 | 43·75 | 40·61 | 45·04 | 44·24 | 38·41 | 44·68 | 42·50 | 52 | 41 | |
| Zn | 118·05 | 120·19 | 120·86 | 120·50 | 120·88 | 116·27 | 118·13 | 124·83 | 118·87 | 126·19 | 126 | 132 | |
| Ga | 23·25 | 23·88 | 23·45 | 23·57 | 23·90 | 23·36 | 23·10 | 24·57 | 23·55 | 24·83 | 21·9 | 23·6 | 24 |
| Rb | 64·33 | 62·13 | 61·85 | 62·02 | 64·70 | 59·28 | 57·71 | 66·34 | 62·39 | 66·68 | 54·6 | 52·5 | 43 |
| Sr | 1336·50 | 1258·79 | 1208·98 | 1226·09 | 1300·00 | 1198·25 | 1205·72 | 1383·73 | 1220·03 | 1317·55 | 937 | 1230·5 | 786 |
| Y | 30·62 | 29·48 | 28·52 | 29·06 | 31·07 | 28·19 | 28·34 | 32·68 | 28·87 | 30·72 | 29·2 | 30·6 | 30·5 |
| Zr | 391·87 | 381·25 | 364·15 | 378·83 | 399·78 | 357·41 | 359·11 | 422·09 | 376·64 | 396·70 | 353 | 357 | 357·6 |
| Nb | 67·28 | 95·55 | 93·08 | 95·93 | 99·89 | 91·64 | 93·24 | 103·97 | 97·55 | 94·55 | 90·2 | 90 | 89·9 |
| Mo | 3·98 | 4·01 | 3·29 | 4·05 | 3·99 | 3·76 | 3·49 | 4·23 | 4·15 | 3·86 | 5·25 | | |
| Sn | 3·12 | 3·13 | 3·23 | 3·19 | 3·15 | 2·97 | 3·13 | 3·33 | 3·19 | 3·39 | 8·8 | | |
| Cs | 1·14 | 1·03 | 0·97 | 1·04 | 1·09 | 0·97 | 0·90 | 1·01 | 1·02 | 1·01 | 0·91 | | |
| Ba | 816·90 | 795·46 | 767·62 | 785·43 | 831·18 | 762·54 | 757·94 | 894·19 | 784·63 | 860·81 | 652 | 775 | 872 |
| La | 66·42 | 64·61 | 62·47 | 64·38 | 67·69 | 61·55 | 61·63 | 72·25 | 63·99 | 66·50 | 59·6 | 74 | 73 |
| Ce | 129·43 | 125·15 | 120·72 | 124·09 | 132·47 | 118·47 | 119·68 | 141·28 | 124·05 | 130·32 | 112 | 125 | 127 |
| Pr | 14·50 | 14·04 | 13·46 | 13·84 | 14·73 | 13·27 | 13·30 | 15·77 | 13·75 | 14·69 | 14·1 | | |
| Nd | 54·48 | 52·47 | 50·54 | 51·52 | 55·54 | 49·81 | 49·95 | 59·28 | 51·61 | 55·40 | 50·7 | 52·88 | 40·56 |
| Sm | 10·53 | 10·18 | 9·86 | 10·06 | 10·70 | 9·74 | 9·81 | 11·49 | 10·00 | 10·85 | 9·9 | 10·32 | 8·45 |
| Eu | 3·31 | 3·25 | 3·15 | 3·19 | 3·40 | 3·13 | 3·14 | 3·61 | 3·18 | 3·43 | 3·13 | | |
| Gd | 9·42 | 9·14 | 8·84 | 8·98 | 9·58 | 8·77 | 8·87 | 10·16 | 8·96 | 9·64 | 8·72 | | |
| Tb | 1·27 | 1·23 | 1·19 | 1·21 | 1·27 | 1·19 | 1·20 | 1·36 | 1·21 | 1·29 | 1·24 | | |
| Dy | 6·41 | 6·22 | 6·03 | 6·13 | 6·48 | 6·00 | 6·00 | 6·91 | 6·12 | 6·51 | 5·98 | | |
| Ho | 1·11 | 1·08 | 1·04 | 1·06 | 1·12 | 1·04 | 1·04 | 1·19 | 1·05 | 1·12 | 1·06 | | |
| Er | 2·63 | 2·53 | 2·44 | 2·48 | 2·63 | 2·42 | 2·42 | 2·81 | 2·49 | 2·62 | 2·52 | | |
| Tm | 0·35 | 0·33 | 0·32 | 0·33 | 0·35 | 0·32 | 0·32 | 0·37 | 0·33 | 0·35 | | | |
| Yb | 1·99 | 1·89 | 1·82 | 1·85 | 1·95 | 1·79 | 1·78 | 2·08 | 1·85 | 1·93 | 1·8 | | |
| Lu | 0·27 | 0·26 | 0·24 | 0·25 | 0·27 | 0·24 | 0·24 | 0·28 | 0·25 | 0·26 | 0·246 | | |
| Hf | 7·77 | 7·60 | 7·25 | 7·50 | 7·87 | 7·19 | 7·25 | 8·41 | 7·49 | 7·97 | 7·21 | | |
| Ta | 2·87 | 4·59 | 4·11 | 4·71 | 4·20 | 4·46 | 4·60 | 5·03 | 4·15 | 4·10 | 5·24 | | |
| Pb | 6·46 | 6·04 | 5·93 | 5·92 | 6·23 | 5·45 | 5·24 | 6·41 | 5·96 | 6·70 | 5·39 | 4·4 | 6 |
| Th | 9·30 | 9·16 | 8·90 | 9·13 | 9·34 | 8·74 | 8·64 | 9·73 | 9·12 | 9·24 | 8·97 | 8·6 | 8 |
| U | 2·41 | 2·23 | 2·08 | 2·24 | 2·25 | 2·15 | 1·92 | 2·39 | 2·22 | 2·12 | 2·15 | 2·5 | 2 |

(continued)

*Table 2: Continued*

| Lithology: | Trachybasalt | | | | | | | | | Limestone | Sandstone | Red clay | Sp. lherzolite |
|---|---|---|---|---|---|---|---|---|---|---|---|---|---|
| Sample: | A001-1 | A001-2 | B007-3 | B011-4 | B011-5 | B021-4 | B021-5 | 963-Ga4 | 2180 | A007-2 | A007-3 | A007-4 | B011-X2 |
| Li | 7·11 | 6·56 | 11·70 | 12·91 | 12·63 | 8·16 | 6·93 | 5·71 | | 17·29 | 9·31 | 10·82 | 2·01 |
| Be | 2·00 | 1·75 | 2·12 | 2·40 | 2·80 | 2·11 | 2·21 | 1·66 | | 0·31 | 0·58 | 3·22 | 0·02 |
| Sc | 18·89 | 19·54 | 15·56 | 15·03 | 17·85 | 18·04 | 17·97 | 21·5 | | 1·79 | 2·84 | 9·38 | 11·18 |
| V | 190·74 | 187·56 | 169·74 | 176·55 | 191·78 | 173·87 | 186·37 | 176 | | 32·05 | 25·41 | 347·05 | 43·95 |
| Cr | 348·16 | 320·70 | 262·65 | 412·41 | 461·47 | 231·78 | 316·00 | 282 | | 33·82 | 75·82 | 85·22 | 2674·39 |
| Mn | 1186·08 | 1198·58 | 1053·11 | 1325·82 | 1290·43 | 1145·77 | 1202·57 | | | 228·97 | 894·82 | 1451·81 | 1044·90 |
| Co | 48·09 | 48·04 | 41·09 | 44·87 | 54·01 | 45·80 | 47·41 | 245 | | 17·23 | 2·88 | 16·07 | 123·89 |
| Ni | 178·07 | 167·50 | 129·77 | 228·14 | 259·81 | 147·69 | 174·19 | 245 | | 61·76 | 2·91 | 39·27 | 2400·41 |
| Cu | 56·01 | 57·88 | 36·94 | 35·93 | 42·97 | 48·95 | 54·59 | 59·9 | | 10·25 | 2·41 | 5·23 | 3·05 |
| Zn | 103·43 | 102·70 | 102·79 | 97·23 | 118·91 | 106·17 | 107·07 | 109·3 | | 11·34 | 15·47 | 111·89 | 38·71 |
| Ga | 21·16 | 20·94 | 20·30 | 18·67 | 23·50 | 21·75 | 21·46 | 19·2 | | 2·74 | 2·97 | 10·67 | 1·07 |
| Rb | 42·27 | 38·71 | 49·82 | 48·95 | 60·94 | 42·83 | 45·19 | 31·4 | | 20·93 | 19·31 | 78·02 | 0·11 |
| Sr | 827·40 | 749·94 | 867·18 | 808·23 | 1075·46 | 820·17 | 912·53 | 561 | | 800·46 | 57·74 | 323·44 | 6·03 |
| Y | 24·18 | 24·07 | 26·19 | 27·61 | 31·45 | 25·29 | 24·74 | 24·3 | | 6·49 | 44·93 | 16·12 | 0·44 |
| Zr | 221·50 | 201·07 | 265·38 | 274·41 | 339·56 | 251·98 | 254·64 | 185 | | 36·11 | 423·20 | 69·13 | 1·14 |
| Nb | 57·24 | 48·63 | 61·09 | 60·93 | 72·10 | 54·64 | 67·45 | 41·7 | | 2·23 | 6·79 | 2·87 | 0·53 |
| Mo | 2·36 | 2·13 | 2·36 | 3·01 | 3·26 | 2·03 | 2·74 | 1·93 | | 0·04 | 0·15 | 1·03 | 0·05 |
| Sn | 2·42 | 2·48 | 2·88 | 2·81 | 3·35 | 2·43 | 2·68 | 9·6 | | 0·61 | 1·41 | 1·28 | b.d. |
| Cs | 0·71 | 0·66 | 1·12 | 1·26 | 1·95 | 0·76 | 0·67 | 0·3 | | 0·91 | 0·99 | 3·93 | 0·00 |
| Ba | 554·08 | 497·46 | 610·06 | 607·07 | 750·07 | 546·70 | 614·38 | 415 | | 53·22 | 91·21 | 124·85 | 2·27 |
| La | 40·27 | 35·26 | 43·70 | 47·87 | 58·45 | 38·61 | 45·51 | 29 | | 8·55 | 17·02 | 18·46 | 0·40 |
| Ce | 78·00 | 69·48 | 87·64 | 97·26 | 116·14 | 74·94 | 88·44 | 57 | | 15·09 | 36·76 | 58·31 | 0·79 |
| Pr | 9·14 | 8·12 | 10·15 | 11·22 | 13·45 | 8·89 | 10·14 | 7 | | 1·80 | 4·14 | 4·97 | 0·09 |
| Nd | 35·42 | 32·04 | 39·54 | 43·61 | 51·25 | 34·42 | 39·09 | 28·1 | | 6·58 | 15·23 | 18·41 | 0·34 |
| Sm | 7·40 | 6·93 | 8·11 | 8·86 | 10·22 | 7·31 | 8·01 | 6·3 | | 1·20 | 3·20 | 3·78 | 0·06 |
| Eu | 2·47 | 2·32 | 2·57 | 2·71 | 3·19 | 2·40 | 2·65 | 2·12 | | 0·25 | 0·45 | 0·80 | 0·02 |
| Gd | 7·06 | 6·75 | 7·45 | 8·07 | 9·23 | 6·94 | 7·47 | 6·14 | | 1·16 | 3·89 | 3·48 | 0·06 |
| Tb | 0·99 | 0·95 | 1·03 | 1·11 | 1·26 | 0·99 | 1·04 | 0·91 | | 0·16 | 0·76 | 0·52 | 0·01 |
| Dy | 5·08 | 4·97 | 5·38 | 5·67 | 6·48 | 5·20 | 5·32 | 4·73 | | 0·89 | 5·54 | 2·98 | 0·06 |
| Ho | 0·90 | 0·89 | 0·96 | 1·00 | 1·15 | 0·94 | 0·93 | 0·87 | | 0·17 | 1·36 | 0·59 | 0·02 |
| Er | 2·12 | 2·12 | 2·31 | 2·41 | 2·75 | 2·30 | 2·18 | 2·16 | | 0·43 | 4·22 | 1·65 | 0·05 |
| Tm | 0·28 | 0·28 | 0·31 | 0·33 | 0·37 | 0·31 | 0·29 | | | 0·06 | 0·69 | 0·27 | 0·01 |
| Yb | 1·57 | 1·60 | 1·78 | 1·85 | 2·10 | 1·76 | 1·60 | 1·6 | | 0·34 | 4·32 | 1·70 | 0·08 |
| Lu | 0·21 | 0·22 | 0·24 | 0·26 | 0·29 | 0·24 | 0·22 | 0·222 | | 0·05 | 0·65 | 0·24 | 0·01 |
| Hf | 4·82 | 4·42 | 5·66 | 5·70 | 7·07 | 5·34 | 5·42 | 4·22 | | 0·94 | 10·36 | 1·87 | 0·02 |
| Ta | 2·76 | 2·21 | 3·04 | 2·75 | 3·18 | 2·66 | 3·28 | 2·47 | | 0·15 | 0·46 | 0·13 | 0·04 |
| Pb | 3·33 | 3·17 | 5·47 | 6·75 | 6·90 | 3·71 | 3·53 | 3·17 | | 4·00 | 5·77 | 20·35 | 0·02 |
| Th | 5·38 | 4·69 | 6·51 | 6·84 | 8·56 | 5·58 | 6·25 | 4·32 | | 3·25 | 7·74 | 9·37 | 0·07 |
| U | 1·30 | 1·13 | 1·57 | 1·67 | 2·00 | 1·34 | 1·49 | 0·69 | | 2·58 | 2·13 | 1·41 | 0·01 |

(continued)

*Table 2: Continued*

| Lithology: | Sp. lherzolite | | | | | Standards | | | | | |
|---|---|---|---|---|---|---|---|---|---|---|---|
| Sample: | B023-4-X3 | B023-4-X2 | B023-4-X1 | B011-X3 | B011-X1 | BHVO 1 av. run | BHVO-1 Racc | BCR 2 av. run | BCR 2 Racc | DNC 1 av. run | DNC 1 Racc |
| Li | 3·73 | 2·10 | 1·34 | 3·03 | 1·20 | 4·82 | 4·90 | 9·91 | 9·30 | 5·03 | 5·08 |
| Be | 0·05 | 0·07 | 0·01 | 0·01 | 0·02 | 1·12 | 1·10 | 2·50 | 2·30 | 0·22 | 0·23 |
| Sc | 6·05 | 12·16 | 10·49 | 4·89 | 10·44 | 30·82 | 31·80 | 32·98 | 33·00 | 31·32 | 31·10 |
| V | 23·73 | 80·44 | 51·99 | 25·37 | 51·85 | 309·60 | 321·00 | 433·92 | 416·00 | 147·16 | 148·00 |
| Cr | 2071·61 | 2831·27 | 4122·80 | 3799·38 | 2402·55 | 305·91 | 289·00 | 15·97 | 18·00 | 305·76 | 285·00 |
| Mn | 833·12 | 888·89 | 850·10 | 817·30 | 938·19 | 1307·97 | 1301·41 | 1533·10 | 1520·00 | 1139·45 | 1161·80 |
| Co | 115·89 | 85·81 | 90·78 | 113·55 | 100·09 | 43·73 | 45·00 | 36·68 | 37·00 | 56·23 | 55·00 |
| Ni | 2375·58 | 1527·16 | 1687·53 | 2325·92 | 1832·39 | 121·61 | 120·00 | 9·53 | 18·00 | 240·90 | 247·00 |
| Cu | 0·34 | 1·84 | 0·74 | b.d. | 2·32 | 129·91 | 136·00 | 20·89 | 19·00 | 91·34 | 96·00 |
| Zn | 35·72 | 38·88 | 38·65 | 41·14 | 32·91 | 144·97 | 105·00 | 114·70 | 127·00 | 55·65 | 66·00 |
| Ga | 0·70 | 3·32 | 1·40 | 0·62 | 1·48 | 21·82 | 21·00 | 22·78 | 23·00 | 14·35 | 15·00 |
| Rb | 0·36 | 0·06 | 0·03 | 0·05 | 0·13 | 10·14 | 9·50 | 51·73 | 48·00 | 3·90 | 4·50 |
| Sr | 7·80 | 16·07 | 1·63 | 5·65 | 4·39 | 447·10 | 390·00 | 377·52 | 346·00 | 156·72 | 195·00 |
| Y | 0·25 | 4·39 | 0·51 | 0·07 | 0·75 | 26·99 | 28·00 | 37·37 | 37·00 | 18·37 | 18·00 |
| Zr | 2·58 | 9·36 | 0·88 | 2·01 | 1·95 | 179·29 | 180·00 | 196·63 | 188·00 | 39·23 | 41·00 |
| Nb | 0·93 | 0·40 | 0·23 | 0·12 | 0·32 | 19·15 | 19·50 | 13·01 | 12·60 | 1·97 | 2·00 |
| Mo | 0·03 | 0·04 | 0·05 | 0·05 | 0·01 | 1·26 | 1·00 | 207·25 | 248·00 | 0·05 | 0·70 |
| Sn | b.d. | 0·14 | 0·01 | 0·06 | b.d. | −0·07 | 2·30 | 3·16 | 2·11 | 1·85 | 2·46 |
| Cs | 0·01 | 0·00 | 0·00 | 0·00 | 0·00 | 0·11 | 0·10 | 1·32 | 1·10 | 0·24 | 0·30 |
| Ba | 7·64 | 1·10 | 0·91 | 3·89 | 1·40 | 137·77 | 133·00 | 716·81 | 683·00 | 108·75 | 118·00 |
| La | 0·65 | 0·30 | 0·18 | 0·26 | 0·19 | 15·16 | 15·50 | 24·80 | 25·00 | 3·66 | 3·53 |
| Ce | 1·41 | 0·98 | 0·22 | 0·44 | 0·43 | 37·92 | 38·00 | 53·23 | 53·00 | 8·21 | 8·19 |
| Pr | 0·17 | 0·18 | 0·02 | 0·05 | 0·06 | 5·38 | 5·45 | 6·83 | 6·80 | 1·11 | 1·10 |
| Nd | 0·60 | 0·94 | 0·12 | 0·15 | 0·25 | 24·30 | 24·70 | 28·17 | 28·00 | 4·92 | 4·86 |
| Sm | 0·09 | 0·34 | 0·04 | 0·02 | 0·07 | 6·12 | 6·17 | 6·57 | 6·70 | 1·44 | 1·40 |
| Eu | 0·03 | 0·14 | 0·01 | 0·01 | 0·02 | 2·07 | 2·06 | 1·98 | 2·00 | 0·60 | 0·60 |
| Gd | 0·07 | 0·50 | 0·05 | 0·02 | 0·09 | 6·23 | 6·22 | 6·77 | 6·80 | 2·03 | 2·00 |
| Tb | 0·01 | 0·11 | 0·01 | 0·00 | 0·02 | 0·96 | 0·95 | 1·07 | 1·07 | 0·39 | 0·39 |
| Dy | 0·05 | 0·73 | 0·07 | 0·01 | 0·11 | 5·33 | 5·25 | 6·37 | 6·41 | 2·76 | 2·76 |
| Ho | 0·01 | 0·17 | 0·02 | 0·00 | 0·03 | 1·01 | 1·00 | 1·32 | 1·33 | 0·65 | 0·65 |
| Er | 0·03 | 0·50 | 0·06 | 0·01 | 0·09 | 2·53 | 2·56 | 3·64 | 3·66 | 1·95 | 1·90 |
| Tm | 0·00 | 0·08 | 0·01 | 0·00 | 0·02 | 0·35 | 0·33 | 0·55 | 0·54 | 0·31 | 0·33 |
| Yb | 0·04 | 0·48 | 0·09 | 0·01 | 0·12 | 2·03 | 1·98 | 3·39 | 3·50 | 2·00 | 1·97 |
| Lu | 0·01 | 0·07 | 0·02 | 0·00 | 0·02 | 0·28 | 0·28 | 0·51 | 0·51 | 0·31 | 0·31 |
| Hf | 0·04 | 0·28 | 0·02 | 0·05 | 0·05 | 4·39 | 4·30 | 4·85 | 4·80 | 1·03 | 1·05 |
| Ta | 0·05 | 0·05 | 0·03 | 0·02 | 0·04 | 1·04 | 1·20 | 0·72 | 0·74 | 0·13 | 0·10 |
| Pb | 0·04 | 0·01 | b.d. | 0·20 | 0·03 | 2·13 | 2·10 | 10·68 | 11·00 | 6·37 | 6·20 |
| Th | 0·12 | 0·02 | 0·04 | 0·04 | 0·04 | 1·23 | 1·26 | 5·92 | 6·20 | 0·25 | 0·22 |
| U | 0·02 | 0·01 | 0·01 | 0·01 | 0·01 | 0·41 | 0·42 | 1·63 | 1·69 | 0·06 | 0·05 |

(continued)

*Table 2: Continued*

| Lithology: | Basanite | | | | | | Trachybasalt | | | | | | Limestone |
|---|---|---|---|---|---|---|---|---|---|---|---|---|---|
| Sample: | A006-2 | A008-3 | A015-1 | A014-2 | A014-2-re | A016-1 | A001-1 | A001-2 | B007-3 | B021-3 | B021-3-re | B021-5 | A007-2 |
| $^{87}Sr/^{86}Sr$ | 0·704084 | 0·704059 | 0·704117 | 0·704050 | | 0·704126 | 0·703996 | 0·704040 | 0·704382 | 0·704185 | 0·704177 | 0·704001 | 0·708628 |
| 2SE | ±12 | ±14 | ±12 | ±14 | | ±16 | ±14 | ±17 | ±14 | ±15 | ±18 | ±17 | ±14 |
| $^{143}Nd/^{144}Nd$ | 0·512793 | 0·51282 | 0·512806 | 0·512818 | 0·512827 | 0·512811 | 0·512806 | 0·512818 | 0·512759 | 0·512806 | 0·512815 | 0·512812 | 0·511606 |
| 2SE | ±9 | ±7 | ±8 | ±6 | ±10 | ±9 | ±10 | ±7 | ±8 | ±6 | ±6 | ±10 | ±13 |
| $\varepsilon_{Nd}$ | 3·0 | 3·6 | 3·3 | 3·5 | 3·7 | 3·4 | 3·3 | 3·5 | 2·4 | 3·3 | 3·5 | 3·4 | −20·1 |
| $^{206}Pb/^{204}Pb$ | 18·546 | 18·522 | 18·518 | 18·528 | | 18·54 | 18·573 | 18·616 | | 18·589 | | 18·535 | 19·591 |
| $^{207}Pb/^{204}Pb$ | 15·61 | 15·603 | 15·605 | 15·61 | | 15·609 | 15·621 | 15·621 | | 15·616 | | 15·614 | 15·845 |
| $^{208}Pb/^{204}Pb$ | 38·872 | 38·796 | 38·799 | 38·821 | | 38·795 | 38·892 | 38·928 | | 38·89 | | 38·847 | 39·666 |

| Lithology: | Sandstone | Sp. lherzolites | | Standards | | | | | | | | |
|---|---|---|---|---|---|---|---|---|---|---|---|---|
| Sample: | A007-3 | B011-X1 | B011-X2 | BCR2 MB | BCR2 | BHVO2 MB | BHVO2 | JNd-1 | JNd-1 | EN-1 | SRM981.120 | SRM981.120 | SRM981.120 |
| $^{87}Sr/^{86}Sr$ | 0·713843 | | 0·704499 | 0·704995 | 0·704978 | 0·703457 | 0·703465 | | | 0·709151 | | | |
| 2SE | ±14 | | ±15 | ±18 | ±19 | ±16 | ±18 | | | ±14 | | | |
| $^{143}Nd/^{144}Nd$ | 0·512063 | | 0·512579 | 0·5126357 | | 0·512983 | | 0·512113 | 0·512121 | | | | |
| 2SE | ±7 | | ±16 | ±8 | | ±8 | | ±8 | ±12 | | | | |
| $\varepsilon_{Nd}$ | −11·2 | | −1·2 | | | | | | | | | | |
| $^{206}Pb/^{204}Pb$ | 19·956 | 19·134 | 18·629 | | 18·758 | | | | | | 16·933 | 16·931 | 16·932 |
| $^{207}Pb/^{204}Pb$ | 15·739 | 15·672 | 15·598 | | 15·617 | | | | | | 15·482 | 15·480 | 15·482 |
| $^{208}Pb/^{204}Pb$ | 40·121 | 39·641 | 39·034 | | 38·721 | | | | | | 36·680 | 36·676 | 36·682 |

| Lithology: | Standards | | | | |
|---|---|---|---|---|---|
| Sample: | SRM981.120 | SRM981.120 | mean | 2SD absolute | 2SD % |
| $^{87}Sr/^{86}Sr$ | | | | | |
| 2SE | | | | | |
| $^{143}Nd/^{144}Nd$ | | | | | |
| 2SE | | | | | |
| $\varepsilon_{Nd}$ | | | | | |
| $^{206}Pb/^{204}Pb$ | 16·935 | 16·936 | 16·93334 | 0·003994 | 0·023584 |
| $^{207}Pb/^{204}Pb$ | 15·485 | 15·487 | 15·48339 | 0·005609 | 0·036223 |
| $^{208}Pb/^{204}Pb$ | 36·690 | 36·695 | 36·68457 | 0·015721 | 0·042855 |

Major elements in wt %, and CIPW normative compositions, with Mg# calculated as $100 \times Mg^{2+}/(Mg^{2+}+Fe^{2+})$. Trace elements in ppm. All analyses were carried out by MC-ICP-MS. Mass bias for Sr and Nd corrected by internal normalization to $^{88}Sr/^{86}Sr = 8{\cdot}37521$ and $^{146}Nd/^{144}Nd = 0{\cdot}7219$; data are reported relative to values of 0·710230 and 0·511860 for the SRM987-Sr and La Jolla-Nd standards, respectively. Typical external precision (2SE; standard error), based on reproducibility of standards, is ±0·000040 (Sr, 2SE) and ±0·000020 (Nd, 2SE). Suffix '-re' denotes result of a repeat run of same Sr–Nd fraction. $\varepsilon_{Nd}$ is calculated relative to $^{143}Nd/^{144}Nd = 0{\cdot}512638$ in modern CHUR. b.d., below detection limit.

element patterns broadly overlap and extend the NVP depleted lherzolite xenolith field. B023-4-X3 shows anomalous lead, whereas B011-X3 has more abundant Cs, Rb, Ba and Th compared with the depleted lherzolite field (Fig. 5d).

The sedimentary lithic fragments collected at location A007 have trace element concentrations typical for sedimentary rocks (not shown). Compared with the basaltic rocks, the sedimentary fragments are notably lower in LREE and Sr, except for the limestone, which is rich in Sr (800 ppm, compared with 1383–827 ppm in the basaltic rocks).

## Sr–Nd–Pb isotopes

$^{87}Sr/^{86}Sr$ and $^{143}Nd/^{144}Nd$ compositions in both magmatic suites are similar and show very small ranges ($^{87}Sr/^{86}Sr$ 0·70399–0·70418, $^{143}Nd/^{144}Nd$ 0·51279–0·51282, $\varepsilon_{Nd}$ +3·0 to +3·6; Table 2). One of the trachybasalts (B007-3, with

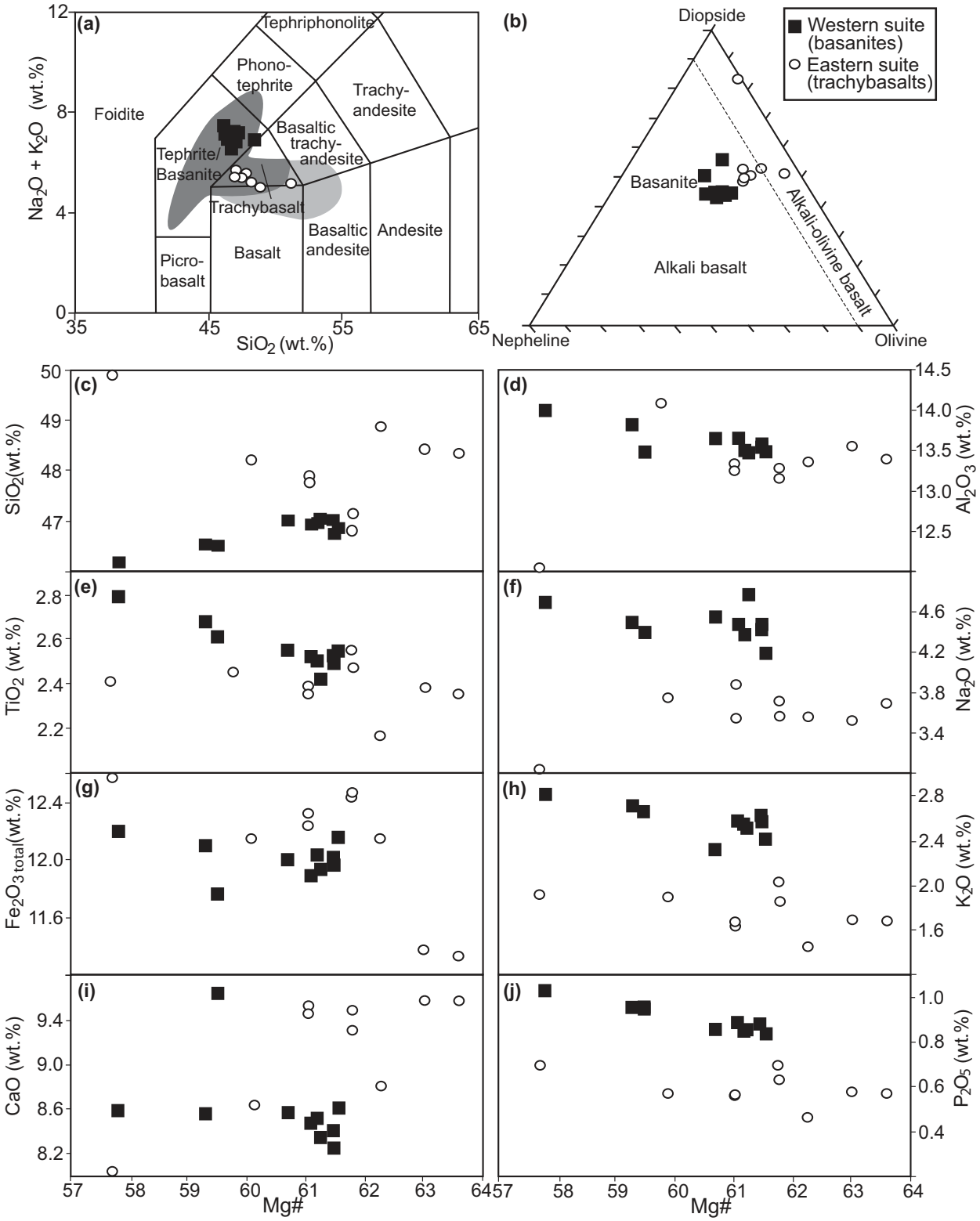


**Fig. 3.** (a) Total alkalis vs silica diagram with the shaded fields representing the alkaline cones (dark grey) and sub-alkaline plains series (light grey); (b) CIPW normative compositions in the Di–Ne–Ol plane of the basalt tetrahedron; (c–j) bivariate plots of major elements vs Mg# [$100 \times Mg^{2+}/(Mg^{2+} + Fe^{2+})$].

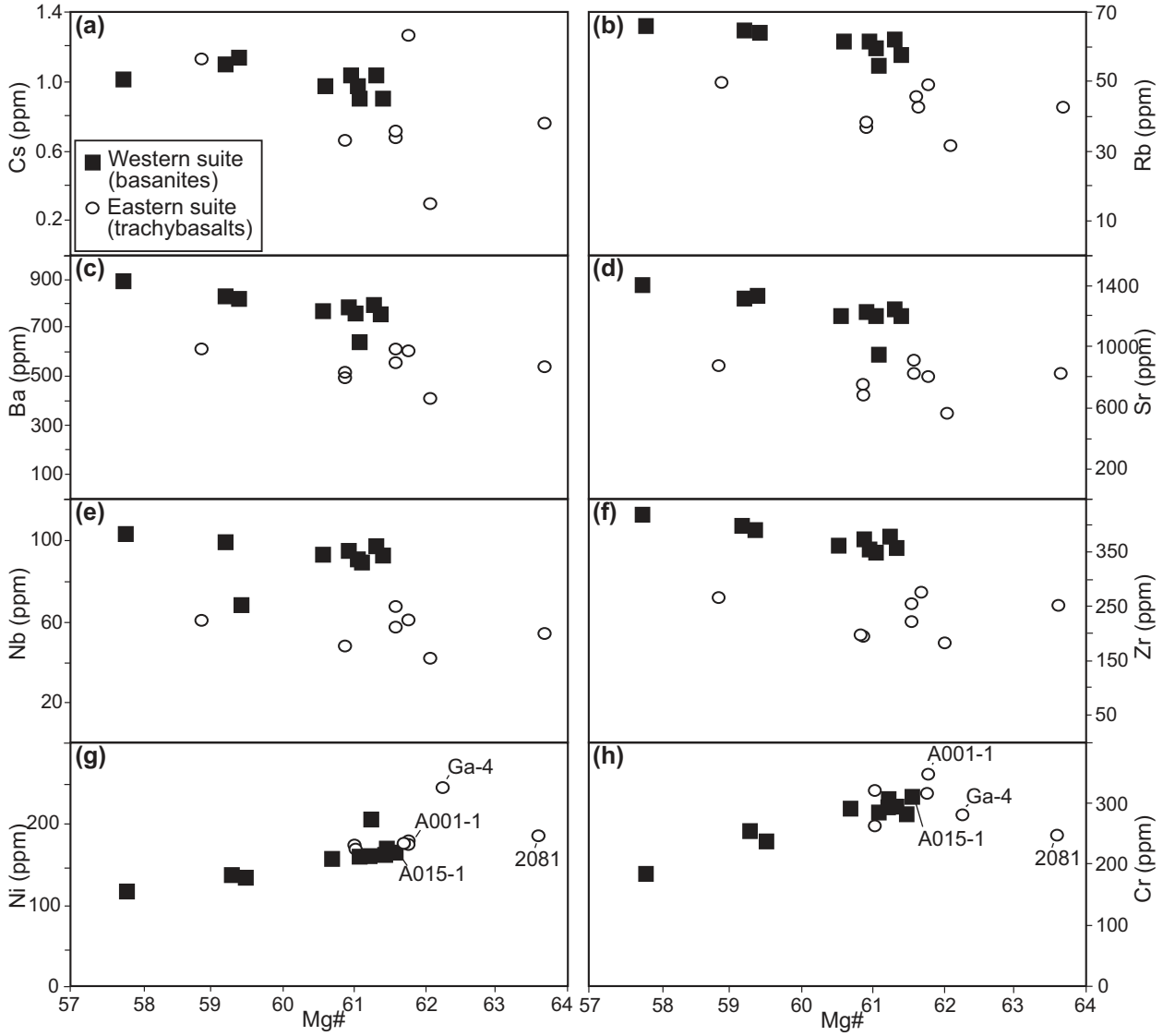


**Fig. 4.** Variation diagrams of selected trace elements vs Mg#.

high Nb and low Cs owing to secondary vesicle infill) has slightly higher $^{87}Sr/^{86}Sr$ (0·70438) and lower $^{143}Nd/^{144}Nd$ (0·512759; $\varepsilon_{Nd}$ +2·4) than the other samples (Fig. 6). Pb isotope compositions also show narrow ranges ($^{206}Pb/^{204}Pb$ 18·518–18·616, $^{207}Pb/^{204}Pb$ 15·603–15·621, $^{208}Pb/^{204}Pb$ 38·795–38·928) although the trachybasalts have resolvably higher ratios than the basanites (Fig. 7). Two lithic clasts, a sandstone and a limestone, have very different Sr–Nd–Pb isotope ratios. The sandstone has high $^{87}Sr/^{86}Sr$ (0·71384) and low $\varepsilon_{Nd}$ [−11·2; model age $T_{Nd}(DM)$ 1·91 Ga] consistent with a provenance from the underlying Palaeozoic basement (Lachlan and Delamerian orogens). The $^{87}Sr/^{86}Sr$ of the limestone clast (0·70863) is consistent with an origin in the marine Oligocene–Miocene Gambier Limestone. The low $\varepsilon_{Nd}$ [−20, replicated; $T_{Nd}(DM)$ 2·2 Ga] in this sample implies the presence of detrital material from the Delamerian Orogen (Turner *et al.*, 1993). The Pb isotope ratios for the clasts are modestly radiogenic, reflecting their age and elevated U/Pb and Th/Pb ratios (Table 2, Fig. 7). Two spinel lherzolite xenoliths have Pb isotope ratios ($^{206}Pb/^{204}Pb$ 19·134, $^{207}Pb/^{204}Pb$ 15·672, $^{208}Pb/^{204}Pb$ 39·641, $^{206}Pb/^{204}Pb$ 18·629, $^{207}Pb/^{204}Pb$ 15·598, $^{208}Pb/^{204}Pb$ 39·034; Table 2) that are distinct from those of their host-rocks, and the Sr–Nd isotopic signature of one of the xenoliths, B011-X2, is slightly more enriched ($^{87}Sr/^{86}Sr$ 0·70449, $^{143}Nd/^{144}Nd$ 0·512579, $\varepsilon_{Nd}$ −1·2) than that of the host rocks (Figs 6 and 7).

The Sr–Nd–Pb isotope compositions of the MGVC basaltic rocks reported here substantially overlap the range of other NVP basalts (McDonough *et al.*, 1985; Ewart *et al.*, 1988;

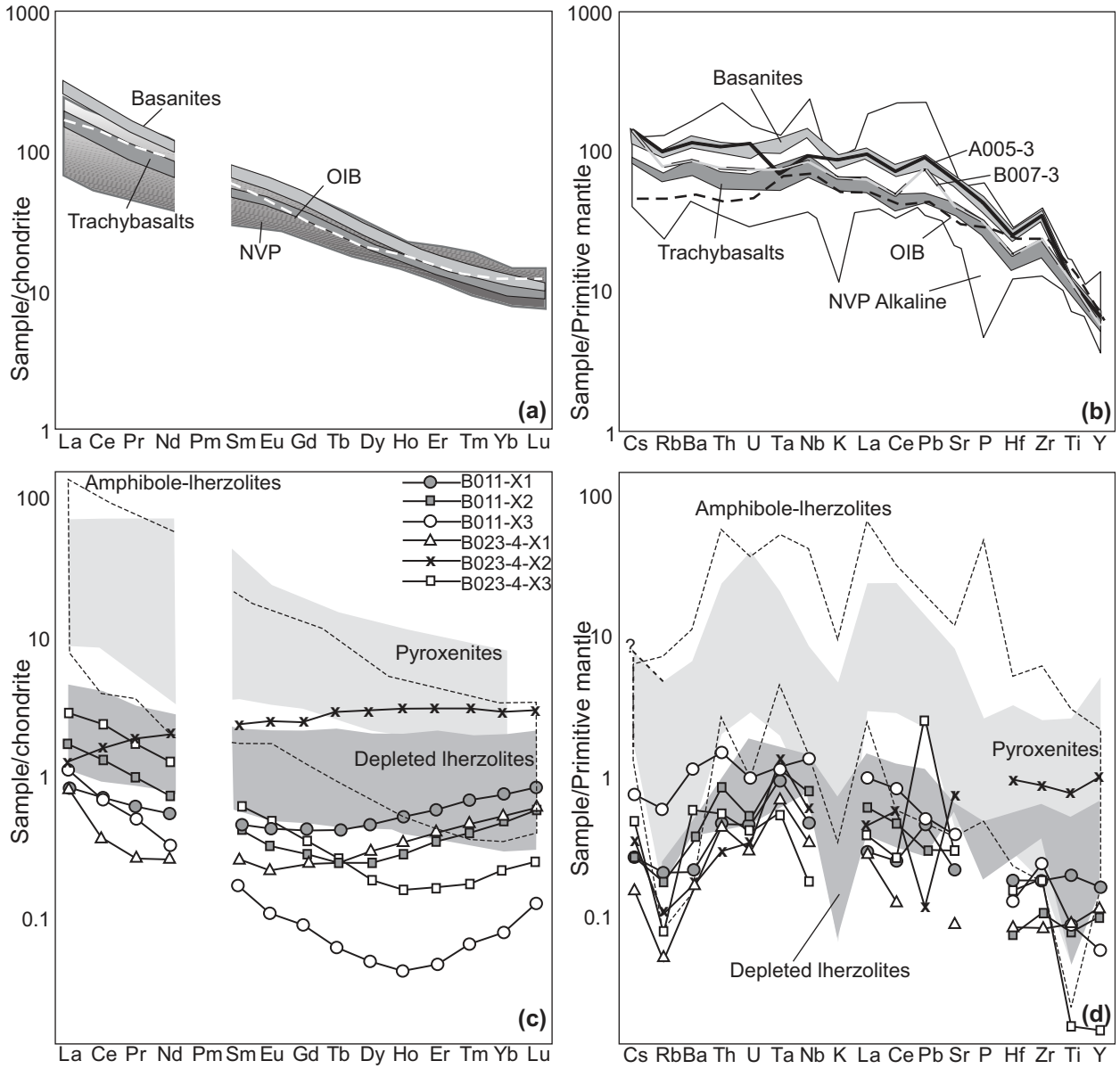


**Fig. 5.** Trace element characteristics of the volcanic rocks: (a) chondrite-normalized rare earth elements; (b) primitive mantle-normalized incompatible elements. The NVP field corresponds to data from the Newer Volcanics Province from the literature referred to in the text; dark grey to light grey transition in (a) corresponds to the increasing alkalinity of the selected samples. Slightly different patterns are observed for samples A005-3 (western suite, low Nb, high Pb) and B007-3 (eastern suite, low Nb, high Cs), which can be attributed to secondary quartz and calcite in vesicles. The trace element abundances of mantle xenoliths from Mt. Gambier are shown in (c) chondrite-normalized rare earth elements, and (d) primitive mantle-normalized incompatible elements. The fields correspond to published data (Green *et al.*, 1968; Griffin *et al.*, 1984, 1988; O'Reilly & Griffin, 1988; Stolz & Davies, 1988; Song, 1994). Normalizing values after Sun & McDonough (1989). Ta values might have been affected by contamination during milling in a carbide tungsten mill; they are plotted only for information.

McBride *et al.*, 2001), including the >6 Ma Euroa mafic suite from Central Victoria (Paul *et al.*, 2005). With a maximum $^{87}Sr/^{86}Sr$ of 0·70418 (for rocks considered unaltered), the MGVC data fit the pattern of $^{87}Sr/^{86}Sr < 0·7042$ for NVP basalts erupted to the west of the Mortlake Discontinuity (Price *et al.*, 1997). New isotopic data for two spinel lherzolites fall within the wide field for lithospheric mantle xenoliths from other localities in southeastern Australia. The Pb isotope composition of xenolith B011-X1 plots close to that of the Enriched Mantle 2 (EM2) mantle end-member of Zindler & Hart (1986). All NVP basalts plot well above the Northern Hemisphere Reference Line (NHRL, Fig. 7) and most mid-ocean ridge basalt (MORB); high $^{208}Pb/^{204}Pb$ relative to $^{206}Pb/^{204}Pb$ is one of the key features of the Dupal anomaly (Dupré & Allègre, 1983; Hart, 1984; Zhang *et al.*, 2001). The data for MGVC and NVP generally, as well as those for

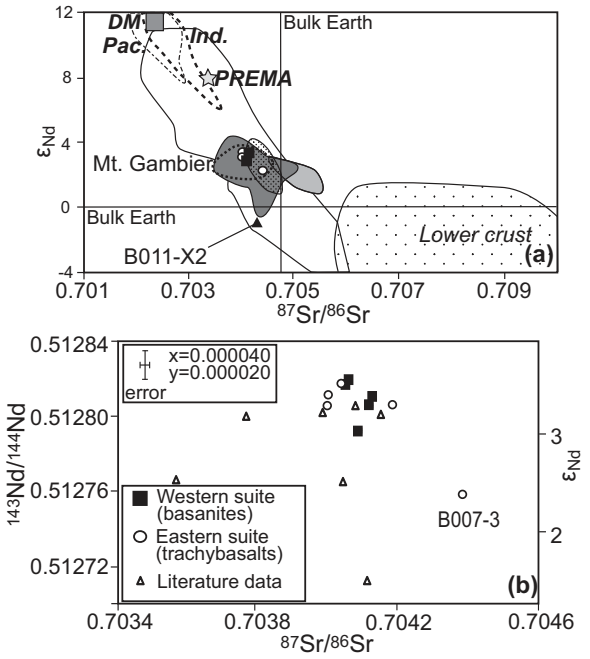


**Fig. 6.** Nd–Sr isotopic compositions for Quaternary basaltic rocks from the Mt Gambier Volcanic Complex. (a) Comparison of the new MGVC data with published data for other samples from the complex (area outlined by dotted line), the alkaline cones series of the NVP (dark grey), the sub-alkaline plains series of the NVP (light grey), the Euroa mafic suite (stippled) and the sub-continental lithospheric mantle (white). Lherzolite xenolith B011-X2 (black triangle). Approximate fields for MORB from the Indian and Pacific Ocean basins, SE Australian lower crust, and the hypothetical Depleted Mantle (DM) and Prevalent Mantle (PREMA) components are shown for comparison. (b) Expanded view of the MGVC data (error bars are 2SD internal). Altered sample B007-3 is clearly offset. Data from other studies (open triangles) cover a larger range than the new data. Data from McDonough *et al.* (1985), Zindler & Hart (1986), Ewart *et al.* (1988), Griffin *et al.* (1988), O'Reilly & Griffin (1988), Stolz & Davies (1988), Song (1994), Hofmann (1997), McBride *et al.* (2001), Foden *et al.* (2002) and Demidjuk *et al.* (2007).

NVP-hosted mantle xenoliths derived from the lithospheric mantle [sub-continental lithospheric mantle (SCLM) field, Fig. 7], show a closer affinity with Indian MORB than with Pacific MORB, consistent with a link between the Dupal signature and the Gondwana mantle (Dupré & Allègre, 1983; Hart, 1984). The xenolith data (SCLM field) also show a well-developed trend towards enriched mantle, in particular the EM2 component (Fig. 7).

# DISCUSSION

## Polymagmatic character of the volcanic complex

Two magmatic suites can be identified at the Mt. Gambier Volcanic Complex: a basanite suite in the west and a trachybasalt suite in the east (Fig. 1c). The former are more alkaline and have higher $P_2O_5$, LREE and incompatible elements, whereas the latter have higher $SiO_2$, MgO, and CaO. The occurrence of these two magmatic suites suggests that the magmatic evolution of MGVC is more complex than previously thought (see Irving & Green, 1976; Foden *et al.*, 2002; Demidjuk *et al.*, 2007).

The geochemical differences between the two suites could be interpreted in two fundamentally different ways, with profound volcanological implications: (1) the MGVC was fed by a single, relatively primitive magma type, which was modified at shallow crustal levels (by fractionation and assimilation) to produce the current compositional spectrum; or (2) the MGVC was fed by two magmas, already distinct in character before reaching crustal depths, giving the complex a polymagmatic character. In the latter case the distinct magma compositions could reflect different mantle sources or variable degrees of melting of a single mantle source. These options are evaluated below.

## Shallow-level wall-rock assimilation and fractionation

Considering the small volume of the erupted volcanic rocks in Mount Gambier ($3{\cdot}25 \times 10^8\,m^3$ tephra, $2{\cdot}37 \times 10^8\,m^3$ DRE magmatic material) (van Otterloo & Cas, 2013), wall-rock assimilation could have been a factor in modifying the primary magma to produce two distinct suites. Crustal assimilation is most likely where magma ascent rates are slow; for example, during temporary storage at crustal levels. However, significant residence of the magma in the crust is unlikely for the MGVC because the presence of mantle xenoliths indicates sufficiently high ascent rates to carry and preserve these inclusions ($>10\,cm\,s^{-1}$; Spera, 1980). Furthermore, key incompatible trace element ratios (e.g. Ce/Pb, Nb/U, Ba/Th, Rb/Nb; Fig. 8; Hofmann *et al.*, 1986; Weaver, 1991) are similar to those for MORB and OIB (Fig. 8a), and indicate no significant crustal influence, although showing affinity to EM2 compositions (Fig. 8b). The exception is Rb/Cs, which shows a wide range in MGVC basalts (30–70; compared with >80 in MORB and OIB; Sun & McDonough, 1989). The lower end of the MGVC Rb/Cs range approaches values more typical of the continental crust (~20). However, low Rb/Cs is common in the alkaline series of the NVP and in xenoliths from southeastern Australian lithospheric mantle (Fig. 5), suggesting that low Rb/Cs may be a characteristic of the mantle source rather than evidence of crustal contamination. Similar low Rb/Cs ratios are found in the Auckland Volcanic Field of New Zealand where crustal contamination has also been ruled out (Smith *et al.*, 2008; McGee *et al.*, 2011, 2012, 2013). Sr–Nd isotope compositions for both suites are tightly clustered and show strong overlap (Fig. 6), making it unlikely that one suite was derived from the other through crustal

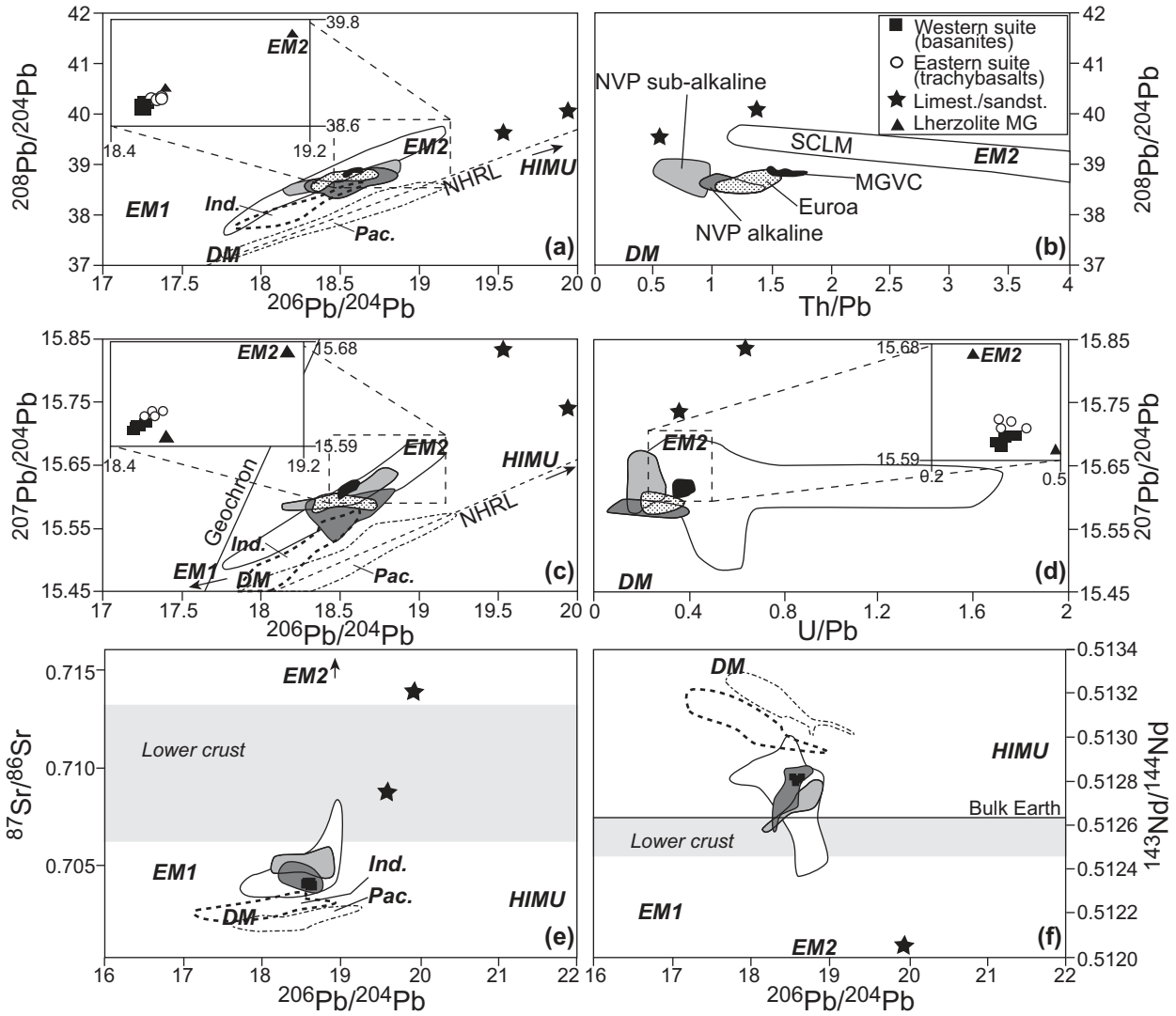


**Fig. 7.** Pb isotope compositions for Quaternary basaltic rocks (black fields in main diagrams; black squares and open circles in insets) and lithic clasts (stars) from the Mt. Gambier Volcanic Complex. (a) $^{208}Pb/^{204}Pb$ vs $^{206}Pb/^{204}Pb$; (b) $^{208}Pb/^{204}Pb$ vs Th/Pb; (c) $^{207}Pb/^{204}Pb$ vs $^{206}Pb/^{204}Pb$; (d) $^{207}Pb/^{204}Pb$ vs U/Pb; (e) $^{87}Sr/^{86}Sr$ vs $^{206}Pb/^{204}Pb$; (f) $^{143}Nd/^{144}Nd$ vs $^{206}Pb/^{204}Pb$. Substantial overlap exists with published results for other basaltic suites from the Newer Volcanic Province: dark grey field, alkaline cones series; light grey field, sub-alkaline plains series; dotted field, Euroa mafic suite, Central Victoria. Published results for xenoliths from the sub-continental lithospheric mantle plot in the large elongated field (no fill). Fields for Pacific and Indian Ocean MORB, the Northern Hemisphere Reference Line (NHRL) and the hypothetical mantle components EM1, EM2, DM and HIMU are shown for comparison. Insets in (a), (c) and (d) show expanded views of the MGVC and two lherzolite xenoliths. Symbols are larger than the analytical errors. Data from Hart (1984), Zindler & Hart (1986), Ewart *et al.* (1988), Stolz & Davies (1988), McBride *et al.* (1996, 2001), Hofmann (1997) and Paul *et al.* (2005).

contamination. The Pb isotope compositions, although also tightly clustered, do appear to define a slight trend towards the more radiogenic lithic clasts (Fig. 7a–d). However, no correlations exist between Pb and Sr–Nd isotopes (Fig. 7e and f). The observed trends in Pb isotopes may instead reflect mixing between melts derived from a heterogeneous mantle source.

Whereas each of the MGVC basaltic suites shows some variation in Mg# (trachybasalts 57·7–63·6; basanites 57·8–61·6), there is relatively little change in major element concentrations relative to Mg#; trace elements also change very little or not at all. The trachybasalt suite shows a scattered negative correlation of $Fe_2O_3$total versus Mg#, but no such trend is observed for the basanite suite. $TiO_2$ correlates negatively with Mg# in the basanite suite but not in the trachybasalts. Only Ni and Cr correlate positively with Mg#, albeit very weakly, which could indicate olivine fractionation. This is examined in Fig. 9, where fractionation trends from the most primitive to most evolved compositions follow the vectors for olivine fractionation. Within-suite variations in Sr and Nd, for example, could be produced by 20% and 30% of olivine

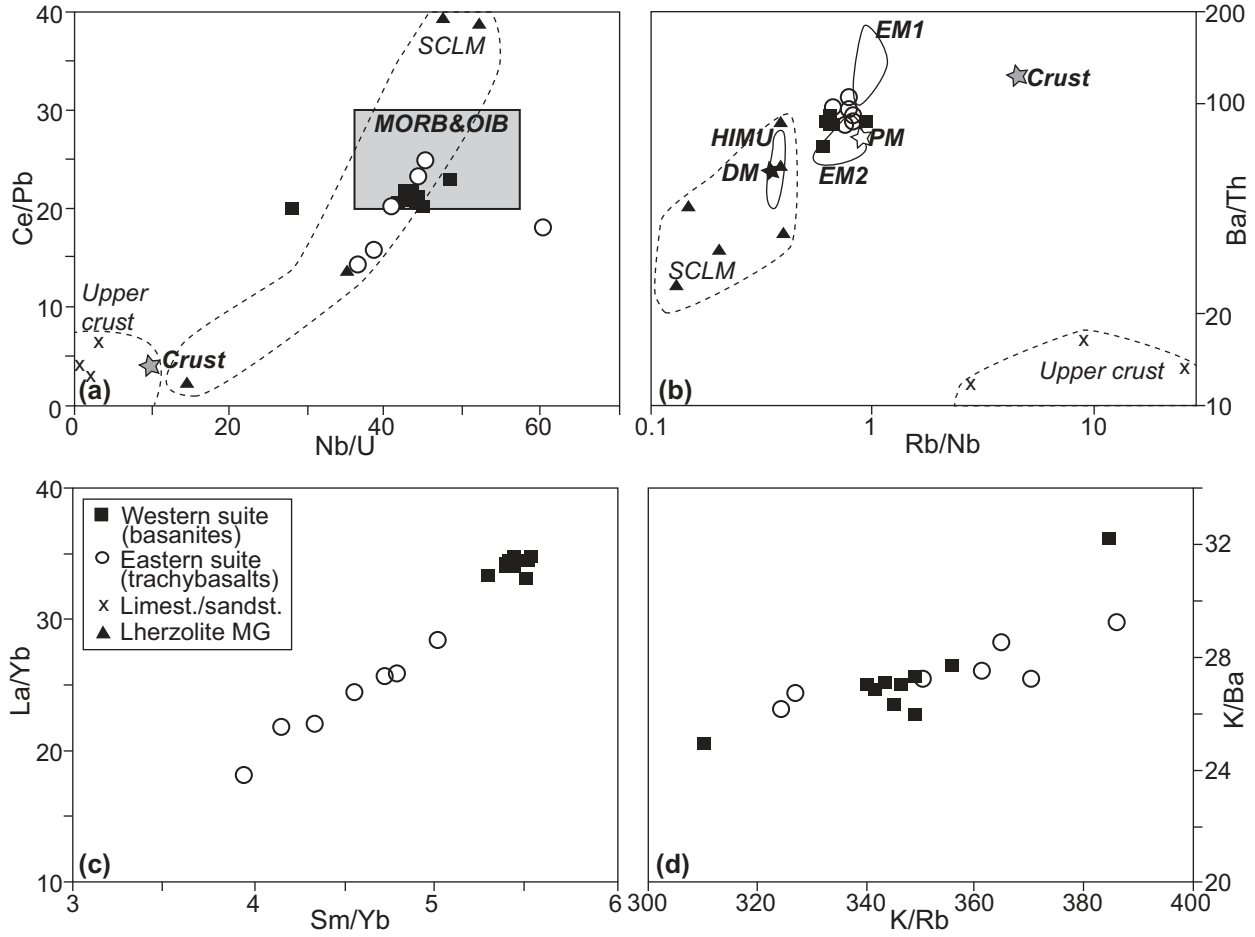


**Fig. 8.** Variation of selected trace-element ratios: (a) Ce/Pb vs Nb/U; (b) Ba/Th vs Rb/Nb; (c) La/Yb vs Sm/Yb; (d) K/Ba vs K/Rb. Fields correspond to data from literature referenced in the text.

fractionation in the western and eastern suites, respectively (Fig. 9b), similar to estimates made by Holt *et al.* (2014). Such large degrees of crystal fractionation are surprising considering the rather homogeneous major and trace element compositions (other than Mg#) and the inferred high magma ascent rates. With such constraints in mind, we suggest that most of the compositional variability in each suite predated shallow-level olivine fractionation; similar observations have been made in studies of other volcanic systems (e.g. Strong & Wolff, 2003; McGee *et al.*, 2012).

Just as within-suite compositional variability is unlikely to result from shallow-level fractionation, such processes also did not produce the differences between the suites. For example, the basanites cannot be produced from a more MgO-rich trachybasalt model parent, because the trachybasalts are higher in $SiO_2$. Although Ca/Al in the basanites is lower than in the trachybasalts (Fig. 9a), the absence of Eu anomalies and plagioclase phenocrysts (Figs 2 and 5) precludes significant plagioclase fractionation. We conclude that shallow-level fractional crystallization cannot have been the main process producing the chemical differences between the two suites.

If differences between the two magmatic suites are not related to crustal assimilation and/or shallow-level fractionation, they must be inherited from their mantle source(s), implying a polymagmatic character for the MGVC. Compositional differences between parental magma batches could be produced by deep-seated differentiation, as at Crater Hill, New Zealand (Smith *et al.*, 2008; McGee *et al.*, 2012), by differences in source composition (e.g. Baker *et al.*, 1997; Németh *et al.*, 2003; Strong & Wolff, 2003; Haase & Renno, 2008; Brenna *et al.*, 2010; Ma *et al.*, 2011) or a combination of the two (McGee *et al.*, 2013).

## Deep-seated processes

### *High-pressure differentiation—modelling bulk crystal extracts*

Assuming that all compositional variation within the two suites was produced by deep-seated crystal–liquid

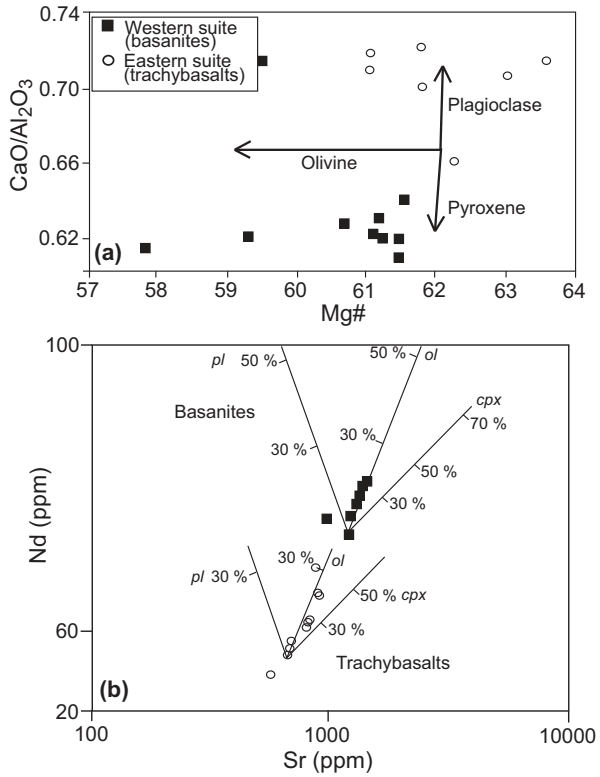


**Fig. 9.** (a) Variation of $CaO/Al_2O_3$ vs Mg# showing that the main fractionating phase in both suites is olivine; (b) vector diagrams of Nd vs Sr; olivine is the major fractionating phase with 20% olivine fractionation occurring in the western basanites compared with 30% in the eastern trachybasalts.

fractionation in the mantle, the relevant bulk partition coefficients ($D$) and bulk mineral extracts can be modelled using the approach of Smith *et al.* (2008) (Fig. 10). Phosphorus is used as a reference element (ref) because it is the major element least compatible with typical mantle mineral assemblages (except for those containing apatite). Using the assumption $D_{ref} = D_P = 0$, $D$ values for REE and other selected trace elements were determined from the power-law regression relationships between these elements and P (Fig. 10a); the exponent in these power regression relationships is equal to $(D_i - 1)/(D_{ref} - 1)$. The resulting model $D$ values (Table 3) can then be compared with published bulk distribution coefficients for garnet, high-pressure clinopyroxene, and kaersutitic and pargasitic amphibole.

The $D$ values of the REE in the trachybasaltic suite largely correspond to those for clinopyroxene and, when considering $D_{LREE}$, these also correspond to the values for garnet. Similar compatibility of the REE is also observed in the Crater Hill basalts of New Zealand (Smith *et al.*, 2008), which has also been associated with deep-seated clinopyroxene ± spinel fractionation. However, in this study the low $D_{Cr}$ of 2·9 for this suite indicates that Cr-spinel cannot be a major fractionating phase. A very low model $D$ value for Ni (1·281) reflects the small range in Ni concentrations and supports the conclusion that olivine is not a dominant fractionating phase. Very low or negative model $D$ values for La, Ce and Nb (Table 3) may reflect open-system behaviour; these elements may have been added during melting or by a deep-seated contaminant.

The model $D_{REE}$ values for the western basanites show little variation from light REE (LREE) to heavy REE (HREE) (Fig. 11), partly resembling those for amphibole and clinopyroxene. The model $D$ values for the LREE strongly resemble those for amphibole. The alkali basalts at Udo Volcano, South Korea, show similar $D$ values (Brenna *et al.*, 2010); these rocks were interpreted to have undergone fractionation of clinopyroxene + olivine ± spinel along with amphibole. The computed $D_{Ni}$ (2·783) is very low and $D_{Nb}$ (0·433) is high, limiting the roles of olivine and clinopyroxene but favouring amphibole. The model results thus suggest that basanite magma genesis could have involved fractionation of amphibole + clinopyroxene ± olivine ± spinel at sub-crustal depths.

The model bulk mineral extract for each suite is obtained via linear extrapolation to a composition of $P_2O_5 = 0$ wt % (Fig. 10b; Smith *et al.*, 2008); this assumes that the fractionating mineral assemblage is P-free. The resulting model extracts (Table 4) are higher in $SiO_2$ than the basalts themselves (trachybasalts 53·5 wt %; basanites 50·6 wt %). The trachybasaltic bulk extract is more CaO-rich than the trachybasaltic suite itself (10·3 wt % vs 9·4 wt %), whereas the opposite is true for the basanites (extract 8·0 wt %; basanites 8·6 wt %). The calculated basanitic extract, however, is richer in MgO relative to the basanites themselves (14·0 wt % vs 8·7 wt %). Both bulk extract compositions are strongly albite-normative, but also rich in normative anorthite and diopside (Table 4). The trachybasaltic crystal extract also contains little olivine and normative hypersthene, which is questionable as alkaline melts are silica-undersaturated and do not fractionate orthopyroxene. The basanitic crystal extract contains much more normative olivine and no hypersthene; this extract is also richer in normative orthoclase and has minor nepheline. Based on these normative compositions and the classification for ultramafic rocks (Le Maitre *et al.*, 2002), the model crystal extracts can be classified as olivine websterite (trachybasalts) and wehrlite (basanites).

The olivine websterite composition for the bulk extract for the trachybasaltic suite is consistent with the prominent role inferred for fractionating clinopyroxene (see above). It shows a good match with the NVP garnet–spinel websterite DR10165 of Adam *et al.* (1992). This xenolith is composed of clinopyroxene (45%), garnet (17%), spinel (7%), orthopyroxene (28%) and amphibole (3%).

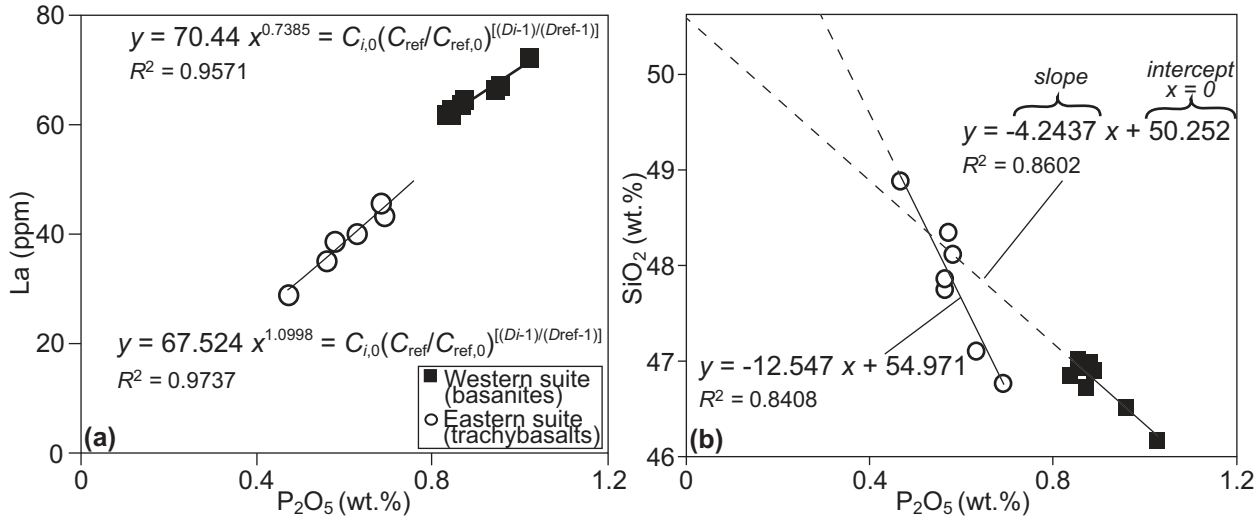


**Fig. 10.** (a) Example of the determination of the bulk partition coefficients ($D_i$) for La. The exponent of the power-law regression is formally equivalent to $(D_i - 1)/(D_{ref} - 1)$, from which $D_i$ can be calculated assuming $D_{ref} = D_P = 0$. (See text for details.) (b) Example of the reconstruction of the bulk crystal extract composition using linear regression. The intercept with $P_2O_5 = 0$ wt % gives the value for the crystal extract composition. Detailed description of these calculations has been given by Smith *et al.* (2008).

The wehrlite bulk extract composition inferred for the basanite suite resembles the composition of the NVP basalts themselves. Ultramafic inclusions with similar compositions hosted in other NVP basalts have been interpreted as cumulates from the basaltic magmas (Griffin *et al.*, 1984, 1988).

The ultramafic xenoliths found in the MGVC do not correlate with the model extract compositions, suggesting that they have no direct genetic relationship with their host magmas but are accidental xenoliths probably sampled from the sub-continental lithospheric mantle during magma ascent. This supports the conclusion that the differentiation processes must have occurred before the magma bodies reached the depth at which the spinel lherzolites were sampled.

In summary, trace element modelling suggests bulk distribution coefficients with similarities to those in potential fractionating phases other than olivine, thus supporting the conclusion that 20–30% olivine fractionation is not probable. The basanitic primitive magma composition was obtained by the fractionation of a peridotite assemblage of amphibole ± clinopyroxene, minor olivine and/or spinel. The most primitive trachybasaltic composition appears to have fractionated a pyroxenite assemblage (clinopyroxene ± garnet) with some amphibole. However, in the context of the trachybasaltic suite inconsistencies remain, such as the high $SiO_2$ content of the inferred bulk crystal extract, the presence of normative hypersthene in an inferred $SiO_2$-undersaturated magma composition, and the anomalous model $D$ values for some highly incompatible elements in the trachybasalts. These indicate that differentiation of the trachybasalt suite occurred in an open system in the presence of a deep-seated contaminant.

### *Primary melt composition and evidence for deep-seated contamination*

The Mg# values for the basanites (57·8–61·6) and the trachybasalts (58·9–63·6) are inconsistent with a primary melt composition that is in equilibrium with a mantle source with olivine of $Fo_{87–88}$ or $Fo_{90}$ for an enriched or depleted mantle source respectively (Frey *et al.*, 1978; Price *et al.*, 1997). A primary melt of this kind would have Mg# ≥68, MgO ≥11 wt % and Ni >300 ppm (Frey *et al.*, 1978), which is very different from observed MGVC compositions. Model primary melt compositions for the MGVC basalts are therefore approximated by extrapolation of their compositional variations to Mg# 70 (Table 5).

The calculated primary melt compositions for both series are basanitic and show major element abundances similar to those of the garnet pyroxenite and wehrlite xenoliths found in the NVP (Griffin *et al.*, 1988). The REE patterns are very similar for both calculated primary melt compositions; these are also very similar to those of the pyroxenite and wehrlite inclusions in the NVP basalts (Griffin *et al.*, 1988; Yaxley *et al.*, 1998). The chondrite-normalized REE patterns show that the only difference is in the degree of LREE enrichment, with the primary melt of the western basanites being more enriched than that of the eastern trachybasalts (Fig. 12). No major difference exists in the HREE content, indicating that the sources for both primary melts had similar amounts of garnet; the major difference is in the degree of melting or deep-seated

*Table 3: The calculated bulk distribution coefficients of the two magmatic suites following the method described by Smith et al. (2008)*

| Element | Trachybasalts $K_D$ | Basanites $K_D$ |
|---|---|---|
| Ba | 0·1664 | 0·2448 |
| Nb | −0·1481 | 0·433 |
| Sr | 0·331 | 0·265 |
| Zr | 0·1846 | 0·185 |
| Ti | 0·6769 | 0·5116 |
| Y | 0·8221 | 0·2738 |
| Zn | 0·9657 | 0·8011 |
| V | 1·108 | 1·213 |
| Ni | 1·281 | 2·783 |
| Sc | 1·618 | 1·661 |
| Cr | 2·9 | 3·377 |
| La | 0·0101 | 0·2615 |
| Ce | −0·0307 | 0·193 |
| Pr | 0·0725 | 0·1838 |
| Nd | 0·1218 | 0·1656 |
| Sm | 0·3483 | 0·232 |
| Eu | 0·4855 | 0·3257 |
| Gd | 0·5558 | 0·3113 |
| Tb | 0·6524 | 0·3572 |
| Dy | 0·727 | 0·3197 |
| Ho | 0·8287 | 0·3193 |
| Er | 0·8724 | 0·268 |
| Tm | 0·9127 | 0·2309 |
| Yb | 0·9264 | 0·2426 |
| Lu | 0·9577 | 0·2306 |
| Cs | 0·9164 | 0·292 |
| Rb | 0·1848 | 0·3245 |
| Th | 0·2636 | 0·269 |
| U | 0·2361 | 0·2921 |

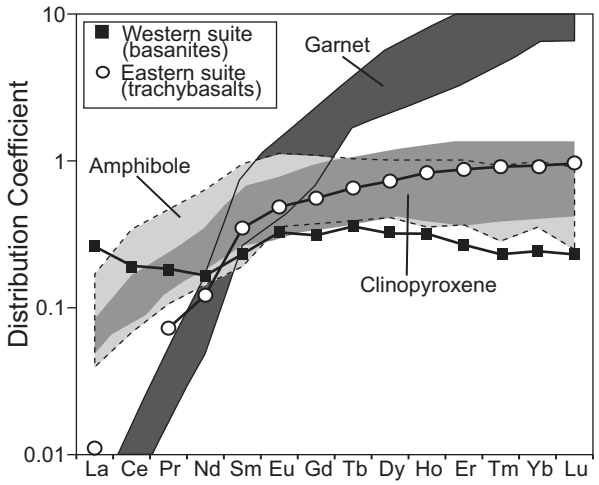


**Fig. 11.** Bulk partition coefficients for the REE calculated from covariation of the elements with $P_2O_5$ in the samples forming the trends of both magmatic suites, compared with literature values for high-pressure clinopyroxene and garnet, after Smith *et al*. (2008) and references therein, as well as high-pressure amphibole. Reference field for the amphibole–melt partitioning is defined by experimental studies including pargasite and/or kaersutite of Dalpe & Baker (1994) and LaTourrette *et al*. (1995) with basanitic glass compositions, Nagasawa (1973) with a trachybasaltic glass composition, and Higuchi & Nagasawa (1969), Mysen (1977, 1978) and Hanson (1980) with basaltic glass compositions; data as cited from Lesnov (2010).

differentiation involving interaction with an LREE-depleted mantle assemblage.

If the assumptions and modelling employed here are realistic, the compositions of inferred primary melt, model bulk crystal extract, and erupted basalt should show plausible relationships on key variation diagrams. We examine such relationships on plots of Ca and Al vs MgO (Fig. 13a and b). Ca and Al are key constituents of clinopyroxene and amphibole, and their concentrations in the modelled and erupted compositions show considerable contrast. Various NVP mantle xenolith suites are also shown in Fig. 13. The Mt. Gambier basalts and the calculated compositions all plot close to the pyroxenite and wehrlite fields, but tend to be lower in MgO. The calculated primary melt composition for the western basanites plots on a line between the most primitive basanitic composition and the related bulk crystal extract (Fig. 13c and d), allowing calculation of mass-balance relations via the Lever Rule. In contrast, the respective geometric relationships for the eastern trachybasalts are not linear. Instead, the most primitive erupted trachybasalt plots on a line between the trachybasalt bulk extract and the inferred primary melt composition of the western basanites. This is also observed when Na and K are plotted versus MgO (Fig. 13e and f). The most primitive trachybasalt plots on a near-linear trend between the model primary melt for the basanites and the olivine websterite extract ($Na_2O$ vs MgO; Fig. 13e), or the primary melt of the eastern trachybasaltic suite could be the result of mixing between these two components ($K_2O$ vs MgO; Fig. 13f). The different behaviour of $K_2O$ in these diagrams probably reflects the incompatibility of K in the mantle assemblage.

To test the validity of the modelled compositions and how these relate, five scenarios were tested by mass-balance models following Stormer & Nicholls (1978) using the program PetroGraph (Petrelli *et al*., 2005), as follows.

(1) Erupted compositions are the result of removal of the calculated bulk extract compositions from the respective primary melts.

*Table 4: The calculated compositions of the bulk crystal extracts of the two magmatic suites following the method described by Smith et al. (2008)*

| Element | Trachybasalts | Basanites |
|---|---|---|
| $SiO_2$ | 53·46 | 50·61 |
| $TiO_2$ | 1·19 | 1·41 |
| $Al_2O_3$ | 13·62 | 11·67 |
| $Fe_2O_3$ | 11·46 | 11·69 |
| total | | |
| MnO | 0·16 | 0·19 |
| MgO | 8·36 | 13·96 |
| CaO | 10·32 | 7·96 |
| $Na_2O$ | 3·47 | 3·60 |
| $K_2O$ | 0·25 | 0·74 |
| Mg# | 61·90 | 72·70 |
| an | 20·81 | 13·46 |
| ab | 29·28 | 28·66 |
| or | 1·48 | 4·37 |
| ne | | 0·93 |
| di | 24·64 | 20·84 |
| hy | 15·71 | |
| ol | 4·43 | 27·14 |
| il | 2·26 | 2·68 |
| mt | 3·68 | 3·76 |

(2) Trachybasalt compositions are derived from the inferred basanite suite primary melt, via removal of the trachybasalt bulk extract.
(3) Trachybasalt primary melt is produced from basanite primary melt via removal of the trachybasalt bulk extract.
(4) Trachybasalt compositions are mixtures of basanites and the trachybasalt bulk extract.
(5) Trachybasalt compositions result from initial fractionation of the basanite bulk extract from the basanitic primary melt; before this process reaches the most primitive basanite, mixing occurs between the fractionating melt and the trachybasalt bulk extract.

The results of the mass-balance modelling of these scenarios are given in Table 6. The western basanitic suite can be explained by fractionation (~53%) of the calculated bulk extract from the related primary melt (scenario 1). Scenarios 4 and 5 fit the results of the modelling, with both showing sum of squares of residuals (SSR) of <2; scenario 5 gives the best solution (SSR <1). The modelling confirms that both magmas originated from a single parental melt; however, one part of the melt differentiated owing to interaction with a garnet pyroxenite composition. During the course of fractionation (52–53%) one part of the melt was altered by interaction with material (0·25–6%) of pyroxenite composition similar to the calculated bulk extract for the eastern trachybasalts. It is important to note that Sr–Nd isotope compositions for garnet pyroxenites similar to those for the NVP basalts have been reported by Griffin *et al.* (1988). This in turn explains why the deep-seated contamination is not reflected in the isotope data for the MGVC basalts.

## Defining the source and melting conditions

### *Partial melting*

The two magmatic suites can be related to a single parental melt as indicated by the discussion above. As mentioned previously, the MGVC basalts are enriched in LILE as well as La and Ce; however, they are depleted in K relative to the other incompatible elements (Fig. 5b). This suggests the presence of a hydrous phase in the source; the increase of K/Rb versus increasing K/Ba indicates residual phlogopite (Fig. 8d; see Brenna *et al.*, 2012). Phlogopite occurs as a minor phase in NVP amphibole-bearing lherzolites (O'Reilly & Griffin, 1985, 1988; Stolz & Davies, 1988); therefore, both amphibole and phlogopite may have coexisted in the source. The presence of garnet is marked by the steep slope of the chondrite-normalized REE patterns, with HREE less than or equal to 10× chondritic.

The effect of garnet in the source can be examined using REE systematics (Fig. 14a). This suggests that REE patterns like those of the MGVC basanites (including the parental melt) could be produced by 3–5% partial melting of a garnet peridotite source with an enriched MORB (E-MORB) composition (Fig. 14a). Similar results are obtained for a Primitive Mantle (PM) composition (not shown). The capacity of NVP amphibole lherzolites, which have trace element patterns similar to those of the basanites (Fig. 5), to generate melts with basanite-like REE patterns is explored in Fig. 14b. The calculations suggest that 4–5% fractional melting of a source similar to an average, modally metasomatized (including amphibole, phlogopite and apatite) lherzolite from the NVP (after O'Reilly & Griffin, 1988; Stolz & Davies, 1988; composition given in the Supplementary Data, which are available for downloading at http://www.petrology.oxfordjournals.org) could produce basanite-like REE patterns

### *Pressure and temperature of melting*

The next step in reconstructing the source and melting conditions is to resolve the depth and temperature of melting. As indicated before, melting occurred at a depth where garnet is stable, an estimated pressure of >1·6–1·7 GPa for SE Australia (O'Reilly & Griffin, 1985, 1996). Following the approach of Hirose & Kushiro (1993)

*Table 5: The reconstructed compositions of the primary melts of the two magmatic suites*

| | Trachybasalts | | | | Basanites | | | |
|---|---|---|---|---|---|---|---|---|
| Element | $R^2$ | Slope | Intercept | $Mg_{70}$ | $R^2$ | Slope | Intercept | $Mg_{70}$ |
| $SiO_2$ | 0·786 | 0·216 | 84·34 | 49·52 | 0·823 | 0·199 | 34·41 | 48·34 |
| $TiO_2$ | 0·404 | −0·028 | 4·63 | 2·15 | 0·886 | −0·075 | 7·07 | 1·84 |
| $Al_2O_3$ | 0·772 | 0·096 | −0·18 | 14·05 | 0·932 | −0·123 | 21·02 | 12·43 |
| $Fe_2O_3$ | 0·417 | −0·185 | 7·45 | 10·58 | 0·365 | −0·045 | 14·71 | 11·54 |
| total | | | | | | | | |
| MnO | 0·728 | 0·003 | −0·11 | 0·18 | 0·103 | 0·001 | 0·09 | 0·18 |
| MgO | 0·748 | 0·227 | −14·77 | 10·64 | 0·953 | 0·323 | −11·30 | 11·29 |
| CaO | 0·802 | 0·193 | −16·80 | 10·84 | 0·235 | −0·044 | 11·09 | 8·03 |
| $Na_2O$ | 0·298 | 0·067 | −0·50 | 4·16 | 0·448 | −0·071 | 8·71 | 3·75 |
| $K_2O$ | 0·171 | −0·042 | 4·39 | 1·44 | 0·485 | −0·077 | 7·21 | 1·84 |
| $P_2O_5$ | 0·091 | −0·012 | 1·34 | 0·50 | 0·910 | −0·046 | 3·66 | 0·46 |
| Mg# | | | | 70·00 | | | | 70·00 |
| an | | | | 15·38 | | | | 11·61 |
| ab | | | | 28·14 | | | | 21·12 |
| or | | | | 8·45 | | | | 10·81 |
| ne | | | | 9·99 | | | | 5·70 |
| di | | | | 28·14 | | | | 20·22 |
| ol | | | | 16·78 | | | | 21·95 |
| il | | | | 4·08 | | | | 3·49 |
| mt | | | | 3·41 | | | | 3·71 |
| ap | | | | 1·16 | | | | 1·07 |
| Ba | 0·249 | −28·805 | 1748·70 | 368·79 | 0·849 | −30·429 | 2638·80 | 508·77 |
| Nb | 0·089 | −2·078 | 22·34 | 63·28 | 0·701 | −2·537 | 250·03 | 72·41 |
| Sr | 0·201 | −42·515 | 807·67 | 839·72 | 0·835 | −46·289 | 4057·70 | 817·47 |
| Zr | 0·471 | −17·026 | 935·82 | 131·52 | 0·756 | −15·013 | 1287·10 | 236·19 |
| Ti | 0·404 | −0·028 | 4·63 | 12850·04 | 0·886 | −0·075 | 7·07 | 11038·81 |
| Y | 0·763 | −0·546 | 61·64 | 19·23 | 0·877 | −1·086 | 95·30 | 19·27 |
| Zn | 0·257 | 1·046 | 81·28 | 108·00 | 0·460 | −1·266 | 196·39 | 107·74 |
| V | 0·448 | 4·390 | −245·36 | 247·47 | 0·352 | 1·589 | 77·53 | 188·76 |
| Ni | 0·707 | 25·270 | −804·94 | 308·06 | 0·972 | 13·873 | −687·74 | 283·37 |
| Sc | 0·656 | 1·216 | −36·22 | 26·35 | 0·747 | 0·485 | −13·36 | 20·56 |
| Cr | 0·444 | 21·739 | −1639·6 | 594·17 | 0·918 | 30·040 | −1544·4 | 558·40 |
| La | 0·170 | −1·885 | 45·74 | 39·88 | 0·830 | −2·384 | 209·12 | 42·22 |
| Ce | 0·216 | −4·193 | 132·19 | 71·61 | 0·839 | −5·091 | 433·84 | 77·51 |
| Pr | 0·236 | −0·450 | 16·79 | 15·92 | 0·845 | −0·573 | 48·70 | 8·60 |
| Nd | 0·249 | −1·649 | 68·46 | 31·12 | 0·866 | −2·224 | 187·23 | 31·56 |
| Sm | 0·272 | −0·271 | 13·63 | 6·62 | 0·875 | −0·403 | 34·65 | 6·41 |
| Eu | 0·138 | −0·053 | 2·23 | 2·52 | 0·864 | −0·113 | 10·11 | 2·18 |
| Gd | 0·233 | −0·182 | 9·34 | 6·79 | 0·867 | −0·323 | 28·70 | 6·11 |
| Tb | 0·237 | −0·018 | 1·34 | 0·95 | 0·871 | −0·041 | 3·70 | 0·85 |
| Dy | 0·421 | −0·119 | 9·03 | 4·60 | 0·874 | −0·216 | 19·33 | 4·19 |
| Ho | 0·692 | −0·022 | 1·98 | 0·77 | 0·887 | −0·037 | 3·34 | 0·73 |
| Er | 0·734 | −0·056 | 6·15 | 1·60 | 0·863 | −0·093 | 8·17 | 1·65 |
| Tm | 0·807 | −0·011 | 0·95 | 0·20 | 0·879 | −0·013 | 1·13 | 0·22 |
| Yb | 0·883 | −0·068 | 6·38 | 0·94 | 0·822 | −0·070 | 6·11 | 1·22 |
| Lu | 0·776 | −0·009 | 0·89 | 0·12 | 0·840 | −0·010 | 0·84 | 0·17 |
| Cs | 0·727 | −0·170 | 6·82 | −0·09 | 0·252 | −0·029 | 2·77 | 0·73 |
| Rb | 0·476 | −3·289 | 158·75 | 31·81 | 0·692 | −1·699 | 183·81 | 42·39 |
| Th | 0·299 | −0·373 | 19·19 | 3·74 | 0·694 | −0·210 | 21·81 | 7·12 |
| U | 0·375 | −0·147 | 6·94 | 0·24 | 0·465 | −0·078 | 7·15 | 1·67 |
| Pb | 0·690 | −0·555 | 37·56 | −1·32 | 0·546 | −0·249 | 20·99 | 3·54 |
| Hf | 0·471 | −0·305 | 18·00 | 3·20 | 0·790 | −0·272 | 23·99 | 4·98 |

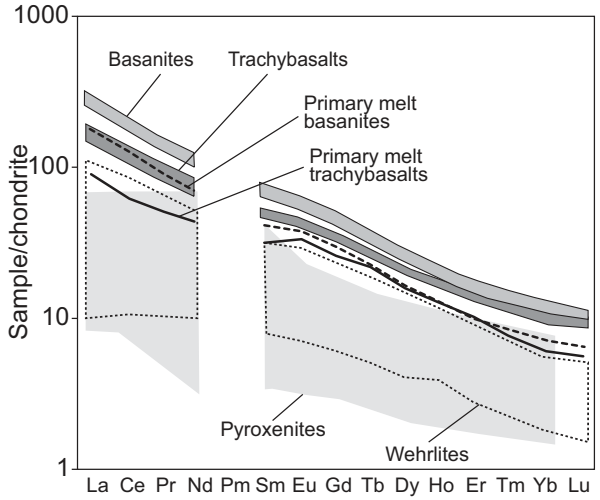


**Fig. 12.** Calculated REE patterns, normalized to chondrite [values from Sun & McDonough (1989)], for the reconstructed primary melt compositions for each magmatic suite. Also shown are the data fields for the two magmatic suites from Fig. 5a.

anhydrous melting of peridotite could produce the required melt compositions at a pressure between 1·5 and 2·0 GPa (Fig. 15). The frequently used silica-activity dependent geothermometer of Lee *et al.* (2009) has not been calibrated for alkaline magma compositions and may overestimate the melting pressure, therefore this model was not used. The model of Wood (2004), for anhydrous melting of fertile peridotite, suggests that the parental melt of the basanites could have been formed by partial melting at $2{\cdot}20 \pm 0{\cdot}33$ GPa (~$80 \pm 12$ km depth) and $1382 \pm 30$°C.

From comparison of these results with the model SE Australian geotherm, the dry peridotite solidus (Hirschmann, 2000), and mantle solidi in the presence of varying amounts of water (Katz *et al.*, 2003) and $H_2O + CO_2$-rich fluids (Wallace & Green, 1988), it is evident that inferred mantle temperatures (1150–1200°C) at the calculated depths are well below those appropriate for the dry peridotite solidus (Fig. 16a). Addition of hydrous and/or $CO_2$-rich fluids would lower melting temperatures or allow melting at higher pressures. At the calculated pressure for the basanites the geotherm crosses the wet solidi with bulk water contents in the source between 0·05 and 0·1 wt % (Fig. 16a).

These results are confirmed by applying the pMELTS model (Ghiorso *et al.*, 2002), where a best fit was found for the production of the parental melt from the average, modally metasomatized lherzolite composition (including 0·37 wt % $H_2O$ and 0·09 wt % $CO_2$) by 4·38% partial melting at a pressure of 2·00 GPa and a temperature of 1220°C [$\Delta f_{O2}$(FMQ) of +4·80]. Basanitic melt produced at these conditions has an $H_2O$ content of 8·45 wt %. The liquidus temperature of this model melt, at 2·20 GPa, is 1230°C [$\Delta f_{O2}$(FMQ) of +2·07]. In comparison, the MGVC basalts erupted with a temperature of $1100 \pm 50$°C and $\Delta f_{O2}$(FMQ) of +2 (van Otterloo, 2012; van Otterloo & Cas, 2013). Conversely, the spinel lherzolite xenoliths in the MGVC volcanic rocks were entrained from a much shallower depth, above the garnet–spinel transition (<1·6 GPa), at a temperature of 930–1100°C and $\Delta f_{O2}$(FMQ) of −2 to −0·5 (Song, 1994).

It is important to note that the southeastern Australian geotherm crosses the garnet pyroxenite solidus (Adam *et al.*, 1992) at 1·7 GPa (~60 km; Fig. 16). Following the geotherm the garnet pyroxenite would be in a partially liquid state at greater pressures and could interact with any passing melt. This pressure therefore is the minimum pressure for deep-seated contamination to occur at the given temperature.

### *Mantle source and processes*

The above pressure–temperature considerations indicate that hydrous and/or $CO_2$-rich fluids could have strongly affected the mantle source and that melting occurred under volatile-present conditions. The next step is to constrain the nature of the fertile mantle source involved and how it has been affected by metasomatism.

The lithosphere–asthenosphere boundary in southeastern Australia, based on seismic tomography models, corresponds to a depth of ~60 km (Fishwick *et al.*, 2008; Ford *et al.*, 2010), which is close to the garnet–spinel transition (1·6–1·7 GPa). A sharp decline in seismic velocity at the base of this thin lithosphere has been explained by the presence of volatile phases and partial melt (compare the garnet pyroxenite mentioned previously) and not just by the thermal gradient (Ford *et al.*, 2010). If, as suggested above, the MGVC basanite melts rose from depths equivalent to a pressure of 2·2 GPa, the melts must be sourced in the asthenosphere and any deep-seated differentiation processes must have occurred before entering the lithosphere. The Sr–Pb–Nd isotope signature of the MGVC basalts, and the NVP basalts in general, suggests the involvement of an asthenospheric mantle source with Indian MORB characteristics (Fig. 7). The isotopic data also suggest a role for a discrete enriched (EM2-like) mantle component (Fig. 7e and f). If the asthenospheric mantle source involved has a MORB-like signature, it is likely that the enriched mantle component may have been derived from a metasomatizing agent.

The effects of the presence of hydrous metasomatic phases on the mantle melting conditions have been widely recognized in various intraplate volcanic fields (e.g. Zhang *et al.*, 2001; Strong & Wolff, 2003; Brenna *et al.*, 2012; McGee *et al.*, 2013). According to the conclusions reached in the present study, $H_2O$ played a significant role during both melting and fractionation, with amphibole being present both in the source and as a fractionating phase. In contrast, the effects of $CO_2$-rich fluids are less well known. These fluids affect melting only if $P > 1{\cdot}7$ GPa; the pressure of 1·7 GPa at ~60 km

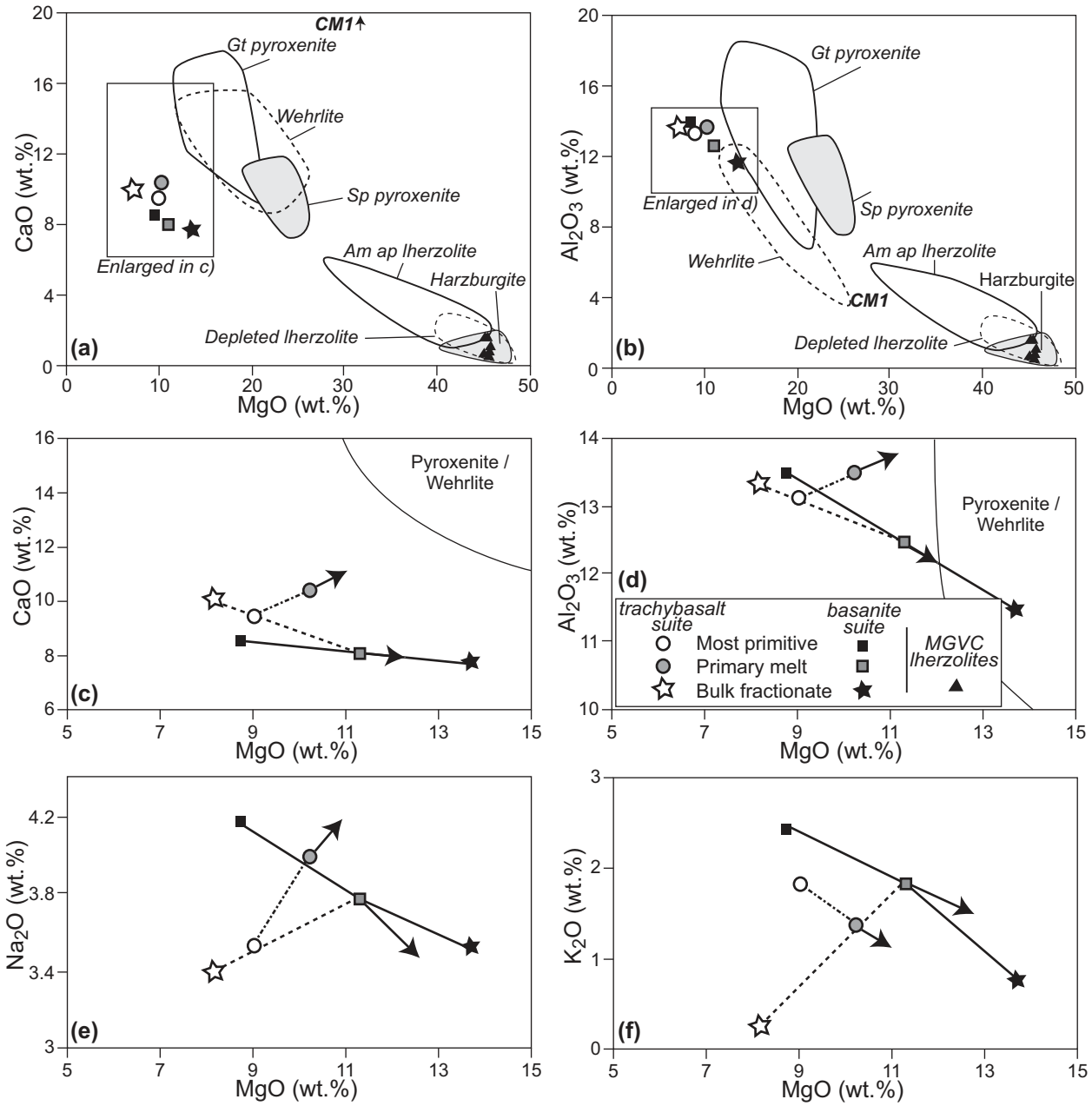


**Fig. 13.** Comparison of the most primitive compositions for both magmatic suites with the reconstructed primary melt and bulk extract compositions and the different mantle xenolith suites from the NVP. CM1 is the sodic dolomitic carbonatite from Yaxley *et al.* (1991). (a) CaO vs MgO; (b) $Al_2O_3$ vs MgO. (c) and (d) show close-up views of (a) and (b), focused on the MGVC compositions. Continuous lines mark the mass-balance relationship between the most primitive basanite and the related primary melt and bulk extract compositions; dotted lines mark hypothetical mass-balance relationships between the trachybasaltic primary melt, bulk extract and most primitive compositions with the primary melt belonging to the basanitic suite. Arrows mark the direction of compositional variation if the primary melt composition has Mg# >70. (e, f) Similar diagrams for $Na_2O$ vs MgO (e) and $K_2O$ vs MgO (f).

corresponding to the decarbonation depth of the sodic dolomitic carbonatite melt of Wallace & Green (1988) and Yaxley *et al.* (1991, 1998) involving the reaction enstatite + dolomite = diopside + forsterite + $CO_2$.

The effects of mantle metasomatism by $CO_2$-rich fluids on the NVP mantle xenoliths were investigated by Yaxley *et al.* (1998) using the hypothetical carbonatite CM1 of Wallace & Green (1988), which has a $CO_2$-free normalized composition of 27·7 wt % MgO, 3·8 wt % $Al_2O_3$ and 41·5 wt % CaO (Fig. 13a and b). In that study the modally and cryptically metasomatized lherzolites, as well as the wehrlites, were considered to be the result of carbonatite

*Table 6: The input and results of the mass balancing modelling using PetroGraph (Petrelli et al., 2005)*

| Scenario 1 Basanites | Start Prim west | Finish A015-1 | Fractionate Bulk west | Obs diff | Calc diff | Residuals |
|---|---|---|---|---|---|---|
| $SiO_2$ | 48·72 | 47·25 | 49·69 | −1·463 | −1·297 | −0·165 |
| $TiO_2$ | 1·86 | 2·57 | 1·38 | 0·712 | 0·63 | 0·082 |
| $Al_2O_3$ | 12·52 | 13·60 | 11·46 | 1·081 | 1·137 | −0·056 |
| $Fe_2O_3$ total | 11·63 | 12·26 | 11·48 | 0·633 | 0·417 | 0·215 |
| MnO | 0·18 | 0·16 | 0·19 | −0·018 | −0·013 | −0·004 |
| MgO | 11·38 | 8·81 | 13·71 | −2·567 | −2·602 | 0·035 |
| CaO | 8·09 | 8·68 | 7·82 | 0·592 | 0·458 | 0·135 |
| $Na_2O$ | 3·78 | 4·22 | 3·54 | 0·443 | 0·364 | 0·079 |
| $K_2O$ | 1·85 | 2·44 | 0·73 | 0·586 | 0·906 | −0·321 |
| Total | 100 | 100 | 100 | | | 0 |
| SSR | | | | | | 0·2121 |
| Wt % phase removed | | | 53·16 | | | |
| Wt % phase added | | | | | | |

| Scenario 1 Trachybasalts | Start Prim east | Finish A001-1 | Fractionate Bulk east | Obs diff | Calc diff | Residuals |
|---|---|---|---|---|---|---|
| $SiO_2$ | 47·82 | 47·43 | 52·26 | −0·392 | −0·895 | 0·503 |
| $TiO_2$ | 2·08 | 2·49 | 1·17 | 0·409 | 0·244 | 0·165 |
| $Al_2O_3$ | 13·56 | 13·25 | 13·32 | −0·317 | −0·013 | −0·303 |
| $Fe_2O_3$ total | 10·22 | 12·56 | 11·21 | 2·342 | 0·251 | 2·091 |
| MnO | 0·17 | 0·16 | 0·15 | −0·012 | 0·002 | −0·013 |
| MgO | 10·28 | 9·11 | 8·17 | −1·166 | 0·174 | −1·339 |
| CaO | 10·47 | 9·56 | 10·09 | −0·911 | −0·098 | −0·813 |
| $Na_2O$ | 4·02 | 3·59 | 3·39 | −0·427 | 0·037 | −0·464 |
| $K_2O$ | 1·39 | 1·86 | 0·25 | 0·473 | 0·299 | 0·174 |
| Total | 100 | 100 | 100 | | | 0 |
| SSR | | | | | | 7·445 |
| Wt % phase removed | | | 18·5 | | | |
| Wt % phase added | | | | | | |

| Scenario 2 Trachybasalts | Start Prim west | Finish A001-1 | Fractionate Bulk east | Obs diff | Calc diff | Residuals |
|---|---|---|---|---|---|---|
| $SiO_2$ | 48·72 | 47·43 | 52·26 | −1·29 | −0·841 | −0·45 |
| $TiO_2$ | 1·86 | 2·49 | 1·17 | 0·632 | 0·229 | 0·402 |
| $Al_2O_3$ | 12·52 | 13·25 | 13·32 | 0·726 | −0·013 | 0·738 |
| $Fe_2O_3$ total | 11·63 | 12·56 | 11·21 | 0·929 | 0·235 | 0·694 |
| MnO | 0·18 | 0·16 | 0·15 | −0·018 | 0·002 | −0·02 |
| MgO | 11·38 | 9·11 | 8·17 | −2·267 | 0·163 | −2·43 |
| CaO | 8·09 | 9·56 | 10·09 | 1·469 | −0·092 | 1·561 |
| $Na_2O$ | 3·78 | 3·59 | 3·39 | −0·19 | 0·035 | −0·226 |
| $K_2O$ | 1·85 | 1·86 | 0·25 | 0·01 | 0·281 | −0·271 |
| Total | 100 | 100 | 100 | | | 0 |
| SSR | | | | | | 9·8588 |
| Wt % phase removed | | | 17·38 | | | |
| Wt % phase added | | | | | | |

(continued)

*Table 6: Continued*

| Scenario 3 | Start | Finish | Fractionate | Obs diff | Calc diff | Residuals |
|---|---|---|---|---|---|---|
| Trachybasalts | Prim west | Prim east | Bulk east | | | |
| $SiO_2$ | 48·72 | 47·82 | 52·26 | −0·898 | −0·646 | −0·253 |
| $TiO_2$ | 1·86 | 2·08 | 1·17 | 0·222 | 0·132 | 0·09 |
| $Al_2O_3$ | 12·52 | 13·56 | 13·32 | 1·043 | 0·035 | 1·007 |
| $Fe_2O_3$ | 11·63 | 10·22 | 11·21 | −1·412 | −0·143 | −1·269 |
| total | | | | | | |
| MnO | 0·18 | 0·17 | 0·15 | −0·007 | 0·003 | −0·01 |
| MgO | 11·38 | 10·28 | 8·17 | −1·101 | 0·306 | −1·407 |
| CaO | 8·09 | 10·47 | 10·09 | 2·38 | 0·055 | 2·325 |
| $Na_2O$ | 3·78 | 4·02 | 3·39 | 0·237 | 0·091 | 0·145 |
| $K_2O$ | 1·85 | 1·39 | 0·25 | −0·463 | 0·166 | −0·629 |
| Total | 100 | 100 | 100 | | | 0 |
| SSR | | | | | | 10·4979 |
| Wt % phase removed | | | 14·52 | | | |
| Wt % phase added | | | | | | |

| Scenario 4 | Start | Finish | Fractionate | Obs diff | Calc diff | Residuals |
|---|---|---|---|---|---|---|
| Trachybasalts | A015-1 | A001-1 | Bulk east | | | |
| $SiO_2$ | 47·25 | 47·43 | 52·26 | 0·172 | 0·275 | −0·103 |
| $TiO_2$ | 2·57 | 2·49 | 1·17 | −0·081 | −0·075 | −0·005 |
| $Al_2O_3$ | 13·60 | 13·25 | 13·32 | −0·356 | 0·004 | −0·36 |
| $Fe_2O_3$ | 12·26 | 12·56 | 11·21 | 0·297 | −0·077 | 0·374 |
| total | | | | | | |
| MnO | 0·16 | 0·16 | 0·15 | −0·001 | −0·001 | 0 |
| MgO | 8·81 | 9·11 | 8·17 | 0·3 | −0·053 | 0·353 |
| CaO | 8·68 | 9·56 | 10·09 | 0·877 | 0·03 | 0·847 |
| $Na_2O$ | 4·22 | 3·59 | 3·39 | −0·633 | −0·011 | −0·622 |
| $K_2O$ | 2·44 | 1·86 | 0·25 | −0·576 | −0·092 | −0·484 |
| Total | 100 | 100 | 100 | | | 0 |
| SSR | | | | | | 1·7416 |
| Wt % phase removed | | | | | | |
| Wt % phase added | | | 5·69 | | | |

| Scenario 5 | Start | Finish | Fractionate | | Obs diff | Calc diff | Residuals |
|---|---|---|---|---|---|---|---|
| Trachybasalts | Prim west | A001-1 | Bulk east | Bulk west | | | |
| $SiO_2$ | 48·72 | 47·43 | 52·26 | 49·69 | −1·29 | −1·176 | −0·114 |
| $TiO_2$ | 1·86 | 2·49 | 1·17 | 1·38 | 0·632 | 0·575 | 0·057 |
| $Al_2O_3$ | 12·52 | 13·25 | 13·32 | 11·46 | 0·726 | 0·935 | −0·209 |
| $Fe_2O_3$ | 11·63 | 12·56 | 11·21 | 11·48 | 0·929 | 0·563 | 0·366 |
| total | | | | | | | |
| MnO | 0·18 | 0·16 | 0·15 | 0·19 | −0·018 | −0·013 | −0·005 |
| MgO | 11·38 | 9·11 | 8·17 | 13·71 | −2·267 | −2·409 | 0·142 |
| CaO | 8·09 | 9·56 | 10·09 | 7·82 | 1·469 | 0·912 | 0·558 |
| $Na_2O$ | 3·78 | 3·59 | 3·39 | 3·54 | −0·19 | 0·026 | −0·217 |
| $K_2O$ | 1·85 | 1·86 | 0·25 | 0·73 | 0·01 | 0·588 | −0·577 |
| Total | 100 | 100 | 100 | 100 | | | 0 |
| SSR | | | | | | | 0·9057 |
| Wt % phase removed | | | | 52·37 | | | |
| Wt % phase added | | | 0·25 | | | | |

The various scenarios are described in the text. SSR, sums of squares.

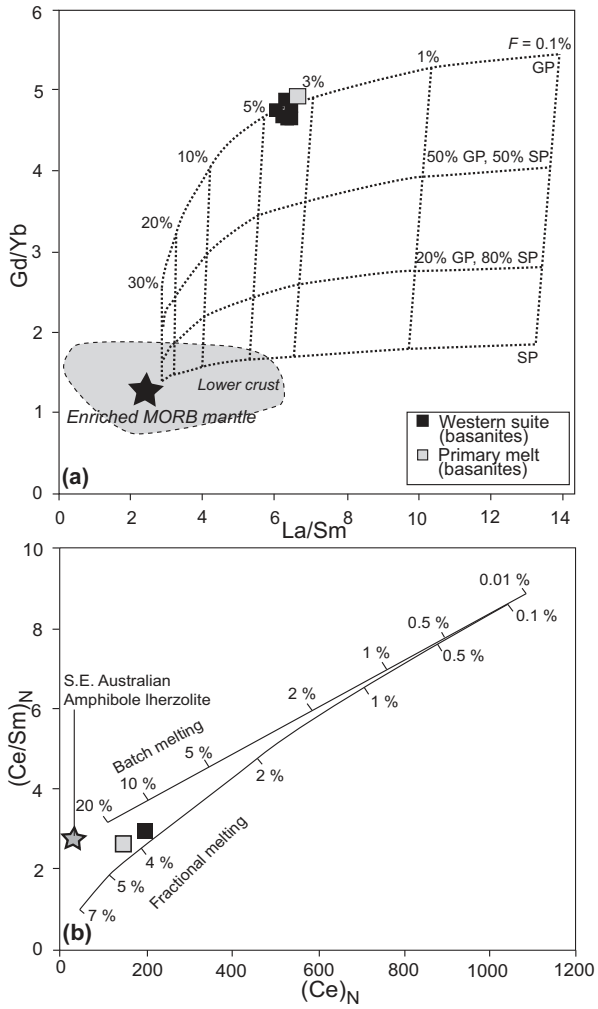


**Fig. 14.** Trace element diagrams to determine source mineralogy and degree of partial melting. (a) Diagram after Song *et al.* (2009), confirming that the basanites were sourced from an enriched garnet peridotite. Enriched MORB from Sun & McDonough (1989); lower crust from Song (1994). GP, garnet peridotite; SP, spinel peridotite; *F*, fraction of melting. (b) Chondrite-normalized Ce/Sm vs Ce vector diagram with partial melting trajectories for batch melting and fractional melting of an amphibole lherzolite source. Amphibole lherzolite composition averaged from O'Reilly & Griffin (1988) (see Supplementary Data for values used).

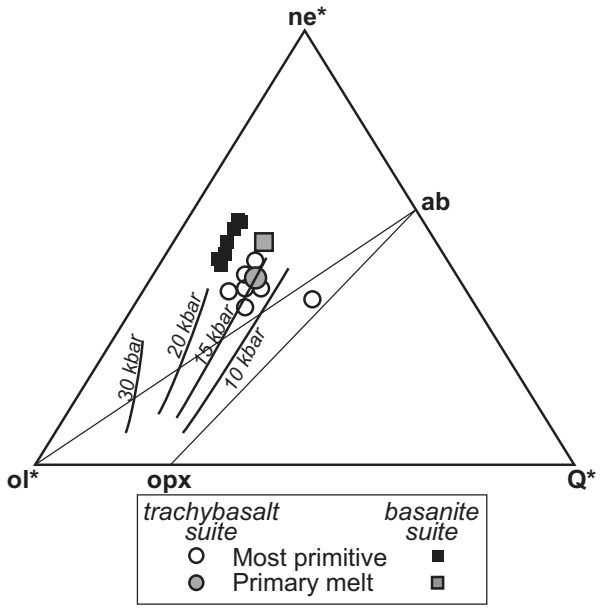


**Fig. 15.** Estimated anhydrous melting pressures for both primary melt compositions as well as the magmatic suites following Hirose & Kishuro (1993). Projection scheme after Irvine & Baragar (1971): $ne^* = ne + 0{\cdot}6ab$; $Q^* = Q + 0{\cdot}4ab + 0{\cdot}25opx$; $ol^* = ol + 0{\cdot}75opx$.

metasomatism; it was argued that melts rich in silica, alkalis and $Al_2O_3$ were extracted in the process. The MGVC basalts could also find their origin in such a metasomatic process; the mantle-derived $CO_2$ sampled in the nearby Caroline-1 well (Chivas *et al.*, 1987) could provide evidence for this.

We draw two preliminary conclusions: (1) MGVC parental melts originated in the asthenosphere and deep-seated differentiation occurred below the base of the lithosphere; (2) metasomatic agents play a major role in the petrogenesis of MGVC and other NVP basalts, imparting a trace element signature enriched in incompatible elements and an 'enriched mantle' (EM2) Sr–Nd–Pb isotopic composition, and lowering the melting temperature of the ambient asthenosperic mantle.

A similar scenario was proposed for the Quaternary Cooktown basalts, northern Queensland, by Zhang *et al.* (2001). Those researchers proposed that the mantle source of these basalts is a mixture between enriched metasomatized mantle and Indian MORB source mantle, extending far to the east of the present-day Indian Ocean basin. In contrast, Finn *et al.* (2005) argued that alkaline magmatic provinces in the SW Pacific (including the NVP and the other eastern Australian basaltic volcanic fields) originate from westward migrating, warm Pacific asthenosphere interacting with metasomatized mantle. The NVP and MGVC isotopic data are more consistent with an Indian MORB or Gondwanan signature than with a Pacific MORB signature.

## Model for the MGVC basalts

Based on the results presented here, combined with modelling of shallow-level and deep-seated differentiation processes, *P–T* estimates and data for mantle xenoliths, we propose the following petrogenetic model for basaltic magmatism in the Mt. Gambier Volcanic Complex (Fig. 16b). The parental melts for the MGVC basalts originate within the asthenospheric mantle at a depth of ~80 km (~2·0–2·2 GPa). Melting was induced by interaction of ambient asthenosphere with Indian MORB isotopic characteristics with hydrous and/or carbonatitic or $CO_2$-rich

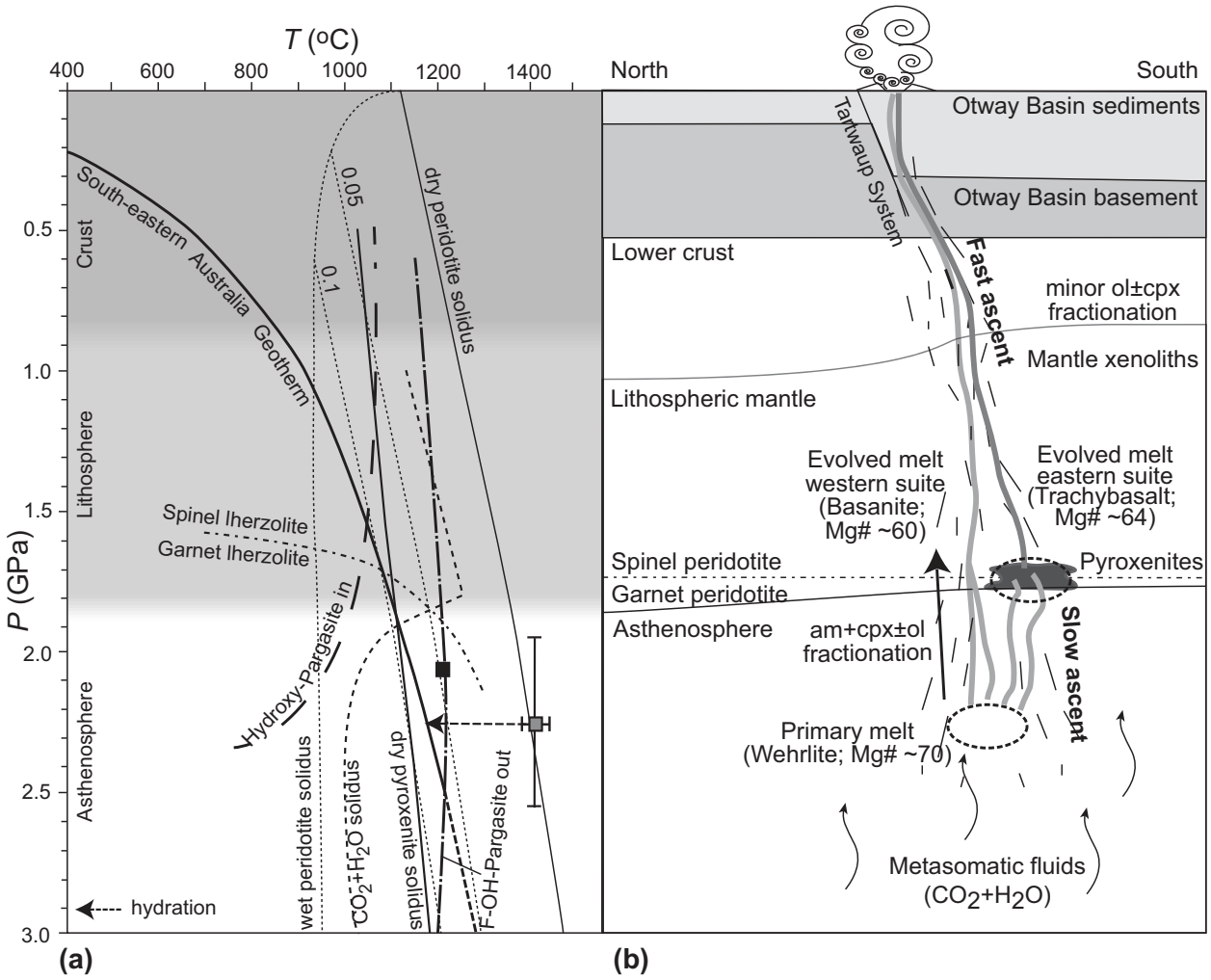


**Fig. 16.** Composite diagram showing (a) the results of the melting models relative to the southeastern Australian geotherm (O'Reilly & Griffin, 1985, 1996), and (b) the model for the magmatic source and evolution of the MGVC basalts. The garnet–spinel transition is marked in (a), along with the dry peridotite solidus after Hirschmann (2000) and the wet solidi with varying water contents after Katz *et al.* (2003). Pargasite stability fields from Foley (1991); $CO_2$ solidus from Falloon & Green (1989); dry pyroxenite solidus from Adam *et al.* (1992). The *P*–*T* calculated conditions for MGVC are from the model of Wood (2004) and pMELTS (Ghiorso *et al.*, 2002) (grey and black squares, respectively). The values according to the model of Wood (2004) follow the dry peridotite solidus; however, the geotherm does not intersect the dry solidus at any point, indicating that a decrease in melting temperature is necessary for melting to occur. The dotted lines indicate the position of the peridotite solidus with 0·05 and 0·1 wt % $H_2O$.

fluids. Low degrees of partial melting (4–5%) produced a basanitic melt that ascended through a network of veins, undergoing deep-seated differentiation by fractionation of an assemblage of amphibole + clinopyroxene ± olivine ± spinel. At the base of the lithosphere (or deeper) some of these melts encountered a garnet pyroxenite body close to its solidus at the asthenosphere–lithosphere boundary (Adam *et al.*, 1992). Chemical interaction with this produced compositional changes, notably higher silica and lower alkalis, LREE and incompatible element contents. The resulting spectrum of melts ascended rapidly through the lithosphere, incorporating lithospheric mantle xenoliths and undergoing very limited olivine-only shallow-level fractionation. Magma ascent appears to have been focused along lithospheric structures of the reactivated Tartwaup Fault System (Fig. 16b). As SE Australia has been under compression for ~10 Myr, zones of transtension need to exist along these reactivated fault structures for the magma to ascend rapidly to the surface.

At the surface, unmodified basanites erupted in the western part of the MGVC, while pyroxenite-contaminated trachybasalts erupted in the east. As can be seen in the simplified stratigraphic representation in Fig. 1c, both magma compositions produced similar volcanic facies as a result of similar eruption styles. The earliest phase, producing the Tenison College Oval maar crater

(van Otterloo & Cas, 2013; van Otterloo *et al.*, 2013), was solely the product of the explosive eruption of the western basanite suite. During the following phases both the western basanites and the eastern trachybasalts produced the remainder of the maar–cone complex. The last phase, however, was again the result of the sole extrusion of western basanites, producing spatter deposits in the Browne's Lake and Valley Lake craters (van Otterloo *et al.*, 2013). This stratigraphic context has two profound implications: both magmatic suites of the MGVC erupted simultaneously, and both suites erupted with similar styles, producing similar volcanic facies.

This model shows that monogenetic volcanism can exhibit great complexity. Next to architectural complexities and changes in eruption styles, petrogenetic complexities can occur. This study shows that a heterogeneous mantle source modified by metasomatic agents can induce melting without the need for an underlying hotspot; it also shows that a single parent melt can differentiate in the asthenosphere by crystal fractionation and contamination processes. The differentiated melt compositions can ascend quickly through the lithosphere and erupt at the same time to produce a single monogenetic volcano with a polymagmatic character. The occurrence of the NVP and the MGVC in a compressive stress regime also highlights that monogenetic volcanism can occur in all tectonic settings.

## CONCLUSIONS

The research presented here adds to our growing understanding that monogenetic volcanic systems can exhibit great complexities in their petrogenesis. The polymagmatic Mt. Gambier Volcanic Complex was formed during the simultaneous eruption of two magma batches that became differentiated at asthenospheric mantle depths, but were derived from a single parent magma. It is argued that differentiation occurred through both deep-seated crystal fractionation as well as contamination. However, although the MGVC erupted two magma compositions, the different volcanic facies related to varying eruption styles were not compositionally controlled.

Another important conclusion from this research is that melting in the mantle beneath SE Australia is not related to the presence of a hotspot or hotline, but is induced by the presence of metasomatic fluids interacting with the shallow asthenosphere. Further research, however, is needed to constrain the origin, timing and dynamics of these metasomatic processes and melting in SE Australia.

## ACKNOWLEDGEMENTS

Ian Smith and Ian Nicholls are thanked for their constructive comments and discussion. Lucy McGee, John Foden and Jan Lindsay are thanked for their careful and constructive reviews. John Gamble is thanked for his careful editorial handling of this paper.

## FUNDING

This research was supported by the Faculty of Science Dean's Scholarship awarded to J.v.O. and discretionary research funds of R.A.F.C.

## SUPPLEMENTARY DATA

Supplementary data for this paper are available at *Journal of Petrology* online.

## REFERENCES

Adam, J., Green, T. H. & Day, R. A. (1992). An experimental study of two garnet pyroxenite xenoliths from the Bullenmerri and Gnotuk Maars of western Victoria, Australia. *Contributions to Mineralogy and Petrology* **111**, 505–514.

Aziz-ur-Rahman, & McDougall, I. (1972). Potassium–argon ages on the Newer Volcanics of Victoria. *Royal Society of Victoria, Proceedings* **85**, 61–69.

Baker, J., Peate, D., Waight, T. & Meyzen, C. (2004). Pb isotopic analysis of standards and samples using a $^{207}Pb$–$^{204}Pb$ double spike and thallium to correct for mass bias with a double-focusing MC-ICP-MS. *Chemical Geology* **211**, 275–303.

Baker, J. A., Menzies, M. A., Thirlwall, M. F. & MacPherson, C. G. (1997). Petrogenesis of Quaternary intraplate volcanism, Sana'a, Yemen: implications for plume–lithosphere interaction and polybaric melt hybridization. *Journal of Petrology* **38**, 1359–1390.

Barbetti, M. & Sheard, M. J. (1981). Palaeomagnetic results from Mounts Gambier and Schank, South Australia. *Geological Society of Australia, Journal* **28**, 385–394.

Barton, C. E. & McElhinny, M. W. (1980). Ages and ashes in lake floor sediment cores from Valley Lake, Mt Gambier, South Australia. *Royal Society of South Australia, Transactions* **104**, 161–165.

Birch, W. D. (2003). *Geology of Victoria. Geological Society of Australia, Special Publication* **23**.

Blackburn, G. (1966). Radiocarbon dates relating to soil development and volcanic ash deposition in South-East South Australia. *Australian Journal of Earth Sciences* **29**, 50–52.

Blackburn, G., Allison, G. B. & Leaney, F. W. J. (1982). Further evidence on the age of the tuff at Mount Gambier, South Australia. *Royal Society of South Australia, Transactions* **106**, 163–167.

Blondes, M. S., Reiners, P. W., Ducea, M. N., Singer, B. S. & Chesley, J. (2008). Temporal–compositional trends over short and long time-scales in basalts of the Big Pine Volcanic Field, California. *Earth and Planetary Science Letters* **269**, 140–154.

Boult, P. J., White, M. R., Pollock, R., Morton, J. G. G., Alexander, E. M. & Hill, A. J. (2002). Lithostratigraphy and environments of deposition. In: Boult, P. J. & Hibburt, J. E. (eds) *The Petroleum Geology of South Australia, Vol. 1: Otway Basin*, 2nd edn. Department of Primary Industries and Resources.

Boyce, J. (2013). The Newer Volcanics Province of southeastern Australia: a new classification scheme and distribution map for eruption centres. *Australian Journal of Earth Sciences* **60**, 449–462.

Brenna, M., Cronin, S., Smith, I., Sohn, Y. & Németh, K. (2010). Mechanisms driving polymagmatic activity at a monogenetic volcano, Udo, Jeju Island, South Korea. *Contributions to Mineralogy and Petrology* **160**, 931–950.

Brenna, M., Cronin, S. J., Smith, I. E. M., Maas, R. & Sohn, Y. K. (2012). How small-volume basaltic magmatic systems develop: a case study from the Jeju Island Volcanic Field, Korea. *Journal of Petrology* **53**, 985–1018.

Cas, R. A. F. & Van Otterloo, J. (2011). Introduction to the IUGG Excursion Guide. In: Cas, R., Blaikie, T., Boyce, J., Hayman, P., Jordan, S., Piganis, F., Prata, G. & Van Otterloo, J. (eds) *Factors that influence varying eruption styles (from magmatic to phreatomagmatic) in intraplate basaltic volcanic provinces: the Newer Volcanics Province of south-eastern Australia. Field trip guide. XXV IUGG General Assembly*. IAVCEI, pp. 7–31.

Cas, R. A. F., Simpson, C. & Sato, H. (1993). *Newer Volcanics Province—Processes and Products of Phreatomagmatic Activity*. Australian Geological Survey Organisation.

Chivas, A. R., Barnes, I., Evans, W. C., Lupton, J. E. & Stone, J. O. (1987). Liquid carbon dioxide of magmatic origin and its role in volcanic eruptions. *Nature* **326**, 587–589.

Clarke, H., Troll, V. R. & Carracedo, J. C. (2009). Phreatomagmatic to Strombolian eruptive activity of basaltic cinder cones: Montaña Los Erales, Tenerife, Canary Islands. *Journal of Volcanology and Geothermal Research* **180**, 225–245.

Dalpe, C. & Baker, D. R. (1994). Partition coefficients for rare-earth elements between calcic amphibole and Ti-rich basanitic glass at 1·5 GPa, 1100°C. *Mineralogical Magazine* **58**, 207–208.

Demidjuk, Z., Turner, S., Sandiford, M., George, R., Foden, J. & Etheridge, M. (2007). U-series isotope and geodynamic constraints on mantle melting processes beneath the Newer Volcanic Province in South Australia. *Earth and Planetary Science Letters* **261**, 517–533.

Demouchy, S., Jacobsen, S. D., Gaillard, F. & Stern, C. H. (2006). Rapid magma ascent recorded by water diffusion profiles in mantle olivine. *Geology* **34**, 429–432.

Doucelance, R. & Manhès, G. (2001). Reevaluation of precise lead isotope measurements by thermal ionization mass spectrometry: comparison with determinations by plasma source mass spectrometry. *Chemical Geology* **176**, 361–377.

Dupré, B. & Allègre, C. J. (1983). Pb–Sr isotope variation in Indian Ocean basalts and mixing phenomena. *Nature* **303**, 142–146.

Elburg, M., Vroon, P., van der Wagt, B. & Tchalikian, A. (2005). Sr and Pb isotopic composition of five USGS glasses (BHVO-2G, BIR-1G, BCR-2G, TB-1G, NKT-1G). *Chemical Geology* **223**, 196–207.

Ewart, A., Chappell, B. W. & Menzies, M. A. (1988). An overview of the geochemical and isotopic characteristics of the eastern Australian Cainozoic volcanic provinces. *Journal of Petrology, Special Lithosphere Issue* 225–273.

Falloon, T. J. & Green, D. H. (1989). The solidus of carbonated, fertile peridotite. *Earth and Planetary Science Letters* **94**, 364–370.

Finlayson, D. M., Finlayson, B., Reeves, C. V., Milligan, P. R., Cockshell, C. D. & Morse, M. P. (1994). The western Otway Basin—a tectonic framework from new seismic, gravity and aeromagnetic data. *Exploration Geophysics* **24**, 493–500.

Finn, C. A., Müller, R. D. & Panter, K. S. (2005). A Cenozoic diffuse alkaline magmatic province (DAMP) in the southwest Pacific without rift or plume origin. *Geochemistry, Geophysics, Geosystems* **6**, Q02005.

Fishwick, S., Heintz, M., Kennett, B. L. N., Reading, A. M. & Yoshizawa, K. (2008). Steps in lithospheric thickness within eastern Australia, evidence from surface wave tomography. *Tectonics* **27**, TC4009.

Foden, J., Song, S. H., Turner, S., Elburg, M., Smith, P. B., Van der Steldt, B. & Van Penglis, D. (2002). Geochemical evolution of lithospheric mantle beneath S.E. South Australia. *Chemical Geology* **182**, 663–695.

Foley, S. (1991). High-pressure stability of the fluor- and hydroxy-end-members of pargasite and K-richterite. *Geochimica et Cosmochimica Acta* **55**, 2689–2694.

Ford, H. A., Fischer, K. M., Abt, D. L., Rychert, C. A. & Elkins-Tanton, L. T. (2010). The lithosphere–asthenosphere boundary and cratonic lithospheric layering beneath Australia from Sp wave imaging. *Earth and Planetary Science Letters* **300**, 299–310.

Frey, F. A. & Green, D. H. (1974). The mineralogy, geochemistry and origin of lherzolite inclusions in Victorian basanites. *Geochimica et Cosmochimica Acta* **38**, 1023–1059.

Frey, F. A. & Prinz, M. (1978). Ultramafic inclusions from San Carlos, Arizona: Petrologic and geochemical data bearing on their petrogenesis. *Earth and Planetary Science Letters* **38**, 129–176.

Frey, F. A., Green, D. H. & Roy, S. D. (1978). Integrated models of basalt petrogenesis: a study of quartz tholeiites to olivine melilitites from south eastern Australia utilizing geochemical and experimental petrological data. *Journal of Petrology* **19**, 463–513.

Genareau, K., Valentine, G., Moore, G. & Hervig, R. (2010). Mechanisms for transition in eruptive style at a monogenetic scoria cone revealed by microtextural analyses (Lathrop Wells volcano, Nevada, U.S.A.). *Bulletin of Volcanology* **72**, 593–607.

Ghiorso, M. S., Hirschmann, M. M., Reiners, P. W. & Kress, V. C. (2002). The pMELTS: A revision of MELTS for improved calculation of phase relations and major element partitioning related to partial melting of the mantle to 3 GPa. *Geochemistry, Geophysics, Geosystems* **3**, 1–35.

Gouramanis, C., Wilkins, D. & De Deckker, P. (2010). 6000 years of environmental changes recorded in Blue Lake, South Australia, based on ostracod ecology and valve chemistry. *Palaeogeography, Palaeoclimatology, Palaeoecology* **297**, 223–237.

Gray, C. M. & McDougall, I. (2009). K–Ar geochronology of basalt petrogenesis, Newer Volcanic Province, Victoria. *Australian Journal of Earth Sciences* **56**, 245–258.

Gray, D. R. & Foster, D. A. (2004). Tectonic evolution of the Lachlan Orogen, southeast Australia: historical review, data synthesis and modern perspectives. *Australian Journal of Earth Sciences* **51**, 773–817.

Green, D. H., Morgan, J. W. & Heier, K. S. (1968). Thorium, uranium and potassium abundances in peridotite inclusions and their host basalts. *Earth and Planetary Science Letters* **4**, 155–166.

Griffin, W. L., Wass, S. Y. & Hollis, J. D. (1984). Ultramafic xenoliths from Bullenmerri and Gnotuk Maars, Victoria, Australia: petrology of a sub-continental crust–mantle transition. *Journal of Petrology* **25**, 53–87.

Griffin, W. L., O'Reilly, S. Y. & Stabel, A. (1988). Mantle metasomatism beneath western Victoria, Australia: II. Isotopic geochemistry of Cr-diopside lherzolites and Al-augite pyroxenites. *Geochimica et Cosmochimica Acta* **52**, 449–459.

Haase, K. M. & Renno, A. D. (2008). Variation of magma generation and mantle sources during continental rifting observed in Cenozoic lavas from the Eger Rift, Central Europe. *Chemical Geology* **257**, 192–202.

Hanson, G. N. (1980). Rare earth elements in petrogenetic studies of igneous systems. *Annual Review of Earth and Planetary Sciences* **8**, 371–406.

Hare, A., Cas, R., Musgrave, R. & Phillips, D. (2005). Magnetic and chemical stratigraphy for the Werribee Plains basaltic lava flowfield, Newer Volcanics Province, southeast Australia: implications for eruption frequency. *Australian Journal of Earth Sciences* **52**, 41–57.

Hart, S. R. (1984). A large-scale isotope anomaly in the Southern Hemisphere mantle. *Nature* **309**, 753–757.

Higuchi, H. & Nagasawa, H. (1969). Partition of trace elements between rock-forming minerals and the host volcanic rocks. *Earth and Planetary Science Letters* **7**, 281–287.

Hillis, R. R., Monte, S. A., Tan, C. P. & Willoughby, D. R. (1995). The contemporary stress field of the Otway Basin, South Australia: implications for hydrocarbon exploration and production. *APEA Journal* **35**, 494–506.

Hirose, K. & Kushiro, I. (1993). Partial melting of dry peridotites at high pressures: Determination of compositions of melts segregated from peridotite using aggregates of diamond. *Earth and Planetary Science Letters* **114**, 477–489.

Hirschmann, M. M. (2000). Mantle solidus: Experimental constraints and the effects of peridotite composition. *Geochemistry, Geophysics, Geosystems* **1**, doi: 10.1029/2000gc000070.

Hofmann, A. W. (1997). Mantle geochemistry: the message from oceanic volcanism. *Nature* **385**, 219–229.

Hofmann, A. W., Jochum, K. P., Seufert, M. & White, W. M. (1986). Nb and Pb in oceanic basalts: new constraints on mantle evolution. *Earth and Planetary Science Letters* **79**, 33–45.

Holt, S. J., Holford, S. P. & Foden, J. (2014). New insights into the magmatic plumbing system of the South Australian Quaternary Basalt province from 3D seismic and geochemical data. *Australian Journal of Earth Sciences* **60**, 797–817.

Irvine, T. J. & Baragar, W. R. (1971). A guide to the chemical classification of the common volcanic rocks. *Canadian Journal of Earth Sciences* **8**, 523–548.

Irving, A. J. (1974). Megacrysts from the Newer Basalts and other basaltic rocks of southeastern Australia. *Geological Society of America Bulletin* **85**, 1503–1514.

Irving, A. J. & Green, D. H. (1976). Geochemistry and petrogenesis of the Newer Basalts of Victoria and South Australia. *Journal of the Geological Society of Australia* **23**, 45–66.

Jensen-Schmidt, B., Cockshell, C. D. & Boult, P. J. (2002). Structural and tectonic setting. In: Boult, P. J. & Hibburt, J. E. (eds) *The Petroleum Geology of South Australia, Vol. 1: Otway Basin*, 2nd edn. Department of Primary Industries and Resources.

Johnson, R. W. (1989). *Intraplate Volcanism in Eastern Australia and New Zealand*. Cambridge University Press.

Jones, R. M., Boult, P. J., Hillis, R. R., Mildrren, S. D. & Kaldi, J. (2000). Integrated hydrocarbon seal evaluation in the Penola Trough, Otway Basin. *APEA Journal* **40**, 194–211.

Joyce, E. B. (1975). Quaternary volcanism and tectonics in southeastern Australia. In: Suggate, R. P. & Cresswell, M. M. (eds) *Quaternary Studies*. Royal Society of New Zealand, pp. 169–178.

Katz, R. F., Spiegelman, M. & Langmuir, C. H. (2003). A new parameterization of hydrous mantle melting. *Geochemistry, Geophysics, Geosystems* **4**, 1073–1091.

LaTourrette, T., Hervig, R. L. & Holloway, J. R. (1995). Trace element partitioning between amphibole, phlogopite, and basanite melt. *Earth and Planetary Science Letters* **135**, 13–30.

Leaney, F. W. J., Allison, G. B., Dighton, J. C. & Trumbore, S. (1995). The age and hydrological history of Blue Lake, South Australia. *Palaeogeography, Palaeoclimatology, Palaeoecology* **118**, 111–130.

Le Bas, M. J., Le Maitre, R. W., Streckeisen, A. L. & Zanettin, B. (1986). A chemical classification of volcanic rocks based the total alkali–silica diagram. *Journal of Petrology* **27**, 745–750.

Lee, C.-T. A., Luffi, P., Plank, T., Dalton, H. & Leeman, W. P. (2009). Constraints on the depths and temperatures of basaltic magma generation on Earth and other terrestrial planets using new thermobarometers for mafic magmas. *Earth and Planetary Science Letters* **279**, 20–33.

Le Maitre, R. W., Streckeisen, A. L., Zanettin, B., Le Bas, M. J., Bonin, B., Bateman, P., Bellieni, G., Dudek, A., Efremova, S., Keller, J., Lameyre, J., Sabine, P. A., Schmid, R., Sørensen, H. & Woolley, A. R. (2002). *Igneous Rocks: A Classification and Glossary of Terms*. Cambridge University Press.

Lesnov, F. P. (2010). *Rare Earth Elements in Ultramafic and Mafic Rocks and their Minerals*. CRC Press–Balkema.

Lesti, C., Giordano, G., Salvini, F. & Cas, R. (2008). Volcano tectonic setting of the intraplate, Pliocene–Holocene, Newer Volcanic Province (southeast Australia): Role of crustal fracture zones. *Journal of Geophysical Research* **113**, doi: 10.1029/2007JB005110.

Lister, G. S. & Etheridge, M. A. (1989). Detachment models for uplift and volcanism in the Eastern Highlands, and their application to the origin of passive margin mountains. In: Johnson, R. W. (ed.) *Intraplate Volcanism in Eastern Australia and New Zealand*. Cambridge University Press, pp. 297–313.

Ma, G. S.-K., Malpas, J., Xenophontos, C. & Chan, G. H.-N. (2011). Petrogenesis of latest Miocene–Quaternary continental intraplate volcanism along the northern Dead Sea Fault System (Al Ghab–Homs Volcanic Field), western Syria: evidence for lithosphere–asthenosphere interaction. *Journal of Petrology* **52**, 401–430.

Maas, R., Kamenetsky, M. B., Sobolev, A. V., Kamenetsky, V. S. & Sobolev, N. V. (2005). Sr, Nd, and Pb isotope evidence for a mantle origin of alkali chlorides and carbonates in the Udachnaya kimberlite, Siberia. *Geology* **33**, 549–552.

Matchan, E. & Phillips, D. (2011). New $^{40}Ar/^{39}Ar$ ages for selected young (<1 Ma) basalt flows of the Newer Volcanic Province, southeastern Australia. *Quaternary Geochronology* **6**, 356–368.

McArthur, J. M., Rio, D., Massari, F., Castradori, F., Bailey, T. R., Thirlwall, M. & Houghton, S. (2006). A revised Pliocene record for marine-$^{87}Sr/^{86}Sr$ used to date an interglacial event recorded in the Cockburn Island Formation, Antarctic Peninsula. *Palaeogeography, Palaeoclimatology, Palaeoecology* **242**, 126–136.

McBride, J. S., Lambert, D. D., Greig, A. & Nicholls, I. A. (1996). Multistage evolution of Australian subcontinental mantle: Re-Os isotopic constraints from Victorian mantle xenoliths. *Geology* **24**, 631–634.

McBride, J. S., Lambert, D. D., Nicholls, I. A. & Price, R. C. (2001). Osmium isotopic evidence for crust–mantle interaction in the genesis of continental intraplate basalts from the Newer Volcanics Province, southeastern Australia. *Journal of Petrology* **42**, 1197–1218.

McDonough, W. F. & McCulloch, M. T. (1987). The southeast Australian lithospheric mantle: isotopic and geochemical constraints on its growth and evolution. *Earth and Planetary Science Letters* **86**, 327–340.

McDonough, W. F., McCulloch, M. T. & Sun, S. S. (1985). Isotopic and geochemical systematics in Tertiary–Recent basalts from southeastern Australia and implications for the evolution of the sub-continental lithosphere. *Geochimica et Cosmochimica Acta* **49**, 2051–2067.

McDougall, I. & Gill, E. D. (1975). Potassium–argon ages from the Quaternary succession in the Warrnambool–Port Fairy area, Victoria, Australia. *Royal Society of Victoria, Proceedings* **87**, 175–178.

McDougall, I., Allsop, H. L. & Chamalaun, F. H. (1966). Isotopic dating of the Newer Volcanics of Victoria, Australia and geomagnetic polarity epochs. *Journal of Geophysical Research* **71**, 6107–6118.

McGee, L., Beier, C., Smith, I. & Turner, S. (2011). Dynamics of melting beneath a small-scale basaltic system: a U–Th–Ra study from Rangitoto volcano, Auckland volcanic field, New Zealand. *Contributions to Mineralogy and Petrology* **162**, 547–563.

McGee, L. E., Millet, M.-A., Smith, I. E. M., Németh, K. & Lindsay, J. M. (2012). The inception and progression of melting in a monogenetic eruption: Motukorea Volcano, the Auckland Volcanic Field, New Zealand. *Lithos* **155**, 360–374.

McGee, L. E., Smith, I. E. M., Millet, M.-A., Handley, H. K. & Lindsay, J. M. (2013). Asthenospheric control of melting processes in a monogenetic basaltic system: a case study of the Auckland Volcanic Field, New Zealand. *Journal of Petrology* **54**, 2125–2153.

Mysen, B. O. (1977). *Partitioning of Cerium, Samarium and Thulium between Pargasite, Garnet Peridotite Minerals and Hydrous Silicate Liquid at High Temperature and Pressure*. Carnegie Institution.

Mysen, B. O. (1978). Experimental determination of rare earth element partitioning between hydrous silicate melt, amphibole and garnet peridotite minerals at upper mantle pressures and temperatures. *Geochimica et Cosmochimica Acta* **42**, 1253–1263.

Nagasawa, H. (1973). Rare-earth distribution in alkali rocks from Oki-Dogo Island, Japan. *Contributions to Mineralogy and Petrology* **39**, 301–308.

Needham, A. J., Lindsay, J. M., Smith, I. E. M., Augustinus, P. & Shane, P. A. (2011). Sequential eruption of alkaline and sub-alkaline magmas from a small monogenetic volcano in the Auckland Volcanic Field, New Zealand. *Journal of Volcanology and Geothermal Research* **201**, 126–142.

Németh, K. (2010). Monogenetic volcanic fields: Origin, sedimentary record, and relationship with polygenetic volcanism. In: Cañón-Tapia, E. & Szakács, A. (eds) *What is a Volcano? Geological Society of America, Special Papers no. 470*, pp. 43–66.

Németh, K., White, J. D. L., Reay, A. & Martin, U. (2003). Compositional variation during monogenetic volcano growth and its implications for magma supply to continental volcanic fields. *Journal of the Geological Society, London* **160**, 523–530.

Newhall, C. G. & Self, S. (1982). The Volcanic Explosivity Index (VEI) an estimate of explosive magnitude for historical volcanism. *Journal of Geophysical Research* **87**, 1231–1238.

Nicholls, I. A. & Joyce, E. B. (1989). East Australian volcanic geology—Victoria and South Australia—Newer Volcanics. In: Johnson, R. W. (ed.) *Intraplate Volcanism in Eastern Australia and New Zealand*. Cambridge University Press, pp. 137–142.

O'Reilly, S. Y. & Griffin, W. L. (1985). A xenolith-derived geotherm for southeastern Australia and its geophysical implications. *Tectonophysics* **111**, 41–63.

O'Reilly, S. Y. & Griffin, W. L. (1988). Mantle metasomatism beneath western Victoria, Australia: I. Metasomatic processes in Cr-diopside lherzolites. *Geochimica et Cosmochimica Acta* **52**, 433–447.

O'Reilly, S. Y. & Griffin, W. L. (1996). 4-D lithosphere mapping: methodology and examples. *Tectonophysics* **262**, 3–18.

Paul, B., Hergt, J. & Woodhead, J. (2005). Mantle heterogeneity beneath the Cenozoic volcanic provinces of central Victoria inferred from trace-element and Sr, Nd, Pb and Hf isotope data. *Australian Journal of Earth Sciences* **52**, 243–260.

Petrelli, M., Poli, G., Perugini, D. & Peccerillo, A. (2005). PetroGraph: A new software to visualize, model, and present geochemical data in igneous petrology. *Geochemistry, Geophysics, Geosystems* **6**, Q07011.

Price, R. C., Gray, C. M. & Frey, F. A. (1997). Strontium isotopic and trace element heterogeneity in the Plains Basalts of the Newer Volcanic Province, Victoria, Australia. *Geochimica et Cosmochimica Acta* **61**, 171–192.

Price, R. C., Gray, C. M., Nicholls, I. A. & Day, R. A. (1988). Cainozoic volcanic rocks. In: Douglas, J. G. & Ferguson, J. A. (eds) *Geology of Victoria*. Geological Society of Australia, pp. 439–451.

Price, R. C., Nicholls, I. A. & Gray, C. M. (2003). Cainozoic igneous activity. In: Birch, W. D. (ed.) *Geology of Victoria. Geological Society of Australia, Special Publication* **23**, 361–375.

Raczek, I., Jochum, K. P. & Hofmann, A. W. (2003). Neodymium and strontium isotope data for USGS reference materials BCR-1, BCR-2, BHVO-1, BHVO-2, AGV-1, AGV-2, GSP-1, GSP-2 and eight MPI-DING reference glasses. *Geostandards Newsletter* **27**, 173–179.

Reiners, P. W. (2002). Temporal–compositional trends in intraplate basalt eruptions: implications for mantle heterogeneity and melting processes. *Geochemistry, Geophysics, Geosystems* **3**, doi: 10.1029/2001GC000250.

Sandiford, M., Wallace, M. & Coblentz, D. (2004). Origin of the *in situ* stress field in south-eastern Australia. *Basin Research* **16**, 325–338.

Sheard, M. J. (1978). Geological history of the Mount Gambier Volcanic Complex, southeast South Australia. *Royal Society of South Australia, Transactions* **102**, 125–139.

Smith, I., Blake, S., Wilson, C. & Houghton, B. (2008). Deep-seated fractionation during the rise of a small-volume basalt magma batch: Crater Hill, Auckland, New Zealand. *Contributions to Mineralogy and Petrology* **155**, 511–527.

Song, S. H. (1994). Geochemical evolution of Phanerozoic lithospheric mantle beneath S.E.South Australia. Ph.D. thesis, University of Adelaide, 328 p.

Song, X.-Y., Keays, R. R., Xiao, L., Qi, H.-W. & Ihlenfeld, C. (2009). Platinum-group element geochemistry of the continental flood basalts in the central Emeishan Large Igneous Province, SW China. *Chemical Geology* **262**, 246–261.

Spera, F. J. (1980). Aspects of magma transport. In: Hargraves, E. B. (ed.) *Physics of Magmatic Processes*. Princeton University Press,, pp. 265–323.

Stolz, A. J. & Davies, G. R. (1988). Chemical and isotopic evidence from spinel lherzolite xenoliths for episodic metasomatism of the upper mantle beneath southeast Australia. *Journal of Petrology, Special Lithosphere Issue* 303–330.

Stormer, J. C. & Nicholls, J. (1978). XLFRAC: a program for the interactive testing of magmatic differentiation models. *Computers and Geosciences* **4**, 143–159.

Strong, M. & Wolff, J. (2003). Compositional variations within scoria cones. *Geology* **31**, 143–146.

Sun, S.-s. & McDonough, W. F. (1989). Chemical and isotopic systematics of oceanic basalts: implications for mantle composition and processes. In: Saunders, A. D. & Norry, M. J. (eds) *Magmatism in the Ocean Basins. Geological Society, London, Special Publications* **42**, 313–345.

Sutherland, F. L. (1991). Cainozoic volcanism, Eastern Australian: a predictive model on migration over multiple 'hotspot' magma sources. In: Williams, M. A. J., DeDeckker, P. & Kershaw, A. P. (eds) *The Cainozoic in Australia: a Re-appraisal of the Evidence. Geological Society of Australia, Special Publication* **18**, 15–43.

Tanaka, T., Togashi, S., Kamioka, H., Amakawa, H., Kagami, H., Hamamoto, T., Yuhara, M., Orihashi, Y., Yoneda, S., Shimizu, H., Kunimaru, T., Takahashi, K., Yanagi, T., Nakano, T., Fujimaki, H., Shinjo, R., Asahara, Y., Tanimizu, M. & Dragusanu, C. (2000). JNdi-1: a neodymium isotopic reference in consistency with LaJolla neodymium. *Chemical Geology* **168**, 279–281.

Turner, S., Foden, J., Sandiford, M. & Bruce, D. (1993). Sm–Nd isotopic evidence for the provenance of sediments from the Adelaide Fold Belt and southeastern Australia with implications for episodic crustal addition. *Geochimica et Cosmochimica Acta* **57**, 1837–1856.

Valentine, G. A. & Gregg, T. K. P. (2008). Continental basaltic volcanoes—Processes and problems. *Journal of Volcanology and Geothermal Research* **177**, 857–873.

Valentine, G. A., Krier, D. J., Perry, F. V. & Heiken, G. (2007). Eruptive and geomorphic processes at the Lathrop Wells scoria cone volcano. *Journal of Volcanology and Geothermal Research* **161**, 57–80.

van Otterloo, J. (2012). Complexity in monogenetic volcanic systems: factors influencing alternating magmatic and phreatomagmatic eruption styles at the 5 ka Mt. Gambier Volcanic Complex, South Australia. Ph.D. thesis, Monash University, 262 p.

van Otterloo, J. & Cas, R. A. F. (2013). Reconstructing the eruption magnitude and energy budgets for the pre-historic eruption of the monogenetic ~5 ka Mt. Gambier Volcanic Complex, south-eastern Australia. *Bulletin of Volcanology* **75**, 1–18.

van Otterloo, J., Cas, R. A. F. & Sheard, M. J. (2013). Eruption processes and deposit characteristics at the monogenetic Mt. Gambier maar complex, SE Australia: implications for alternating magmatic and phreatomagmatic activity. *Bulletin of Volcanology* **75**, 737–758.

Veevers, J. J. (1986). Break-up of Australia and Antarctica estimated as mid-Cretaceous (95 ± 5 Ma) from magnetic and seismic data at the continental margin. *Earth and Planetary Science Letters* **77**, 91–99.

Vogel, D. C. & Keays, R. R. (1997). The petrogenesis and platinum-group element geochemistry of the Newer Volcanic Province, Victoria, Australia. *Chemical Geology* **136**, 181–204.

Walker, G. P. L. (1993). Basaltic-volcano systems. In: Prichard, H. M., Alabaster, T., Harris, N. B. W. & Neary, C. R. (eds) *Magmatic Processes and Plate Tectonics. Geological Society, London, Special Publications* **76**, 3–38.

Wallace, M. E. & Green, D. H. (1988). An experimental determination of primary carbonatite magma composition. *Nature* **335**, 343–346.

Weaver, B. L. (1991). The origin of ocean island basalt end-member compositions: trace element and isotopic constraints. *Earth and Planetary Science Letters* **104**, 381–397.

Weis, D., Kieffer, B., Maerschalk, C., Barling, J., De Jong, J., Williams, G., Hanano, D., Pretorius, W., Mattielli, N., Scoates, J. S., Goolaerts, A., Friedman, R. & Mahoney, J. B. (2006). High-precision isotopic characterization of USGS reference materials by TIMS and MC-ICP-MS. *Geochemistry, Geophysics, Geosystems* **7**, doi: 10.1029/2006GC001283.

Wellman, P. (1974). Potassium–argon ages on the Cainozoic volcanic rocks of Eastern Victoria, Australia. *Journal of the Geological Society of Australia* **21**, 359–376.

Wellman, P. (1983). Hotspot volcanism in Australia and New Zealand: Cainozoic and mid-Mesozoic. *Tectonophysics* **96**, 225–243.

Wellman, P. & McDougall, I. (1974). Cainozoic igneous activity in eastern Australia. *Tectonophysics* **23**, 49–65.

Whitehead, P. W. (1991). The geology and geochemistry of Mt Napier and Mt Rouse, western Victoria. In: Williams, M. A. J., DeDeckker, P. & Kershaw, A. P. (eds) *The Cainozoic in Australia: a Re-appraisal of the Evidence. Geological Society of Australia, Special Publication* **18**, 309–320.

Wood, B. J. (2004). Melting of fertile peridotite with variable amounts of $H_2O$. In: Sparks, R. S. J. & Hawkesworth, C. J. (eds) *The state of the planet: frontiers and challenges in geophysics. Geophysical Monograph 125.* American Geophysical Union, pp. 69–80.

Woodhead, J. D. & Hergt, J. M. (1997). Application of the 'double spike' technique to Pb-isotope geochronology. *Chemical Geology* **138**, 311–321.

Yaxley, G. M., Crawford, A. J. & Green, D. H. (1991). Evidence for carbonatite metasomatism in spinel peridotite xenoliths from western Victoria, Australia. *Earth and Planetary Science Letters* **107**, 305–317.

Yaxley, G. M., Green, D. H. & Kamenetsky, V. (1998). Carbonatite metasomatism in the southeastern Australian lithosphere. *Journal of Petrology* **39**, 1917–1930.

Yoder, H. S. & Tilley, C. E. (1962). Origin of basalt magmas: an experimental study of natural and synthetic rock systems. *Journal of Petrology* **3**, 342–532.

Zhang, M., Stephenson, P. J., O'Reilly, S. Y., McCulloch, M. T. & Norman, M. (2001). Petrogenesis and geodynamic implications of Late Cenozoic basalts in north Queensland, Australia: trace-element and Sr–Nd–Pb isotope evidence. *Journal of Petrology* **42**, 685–719.

Zindler, A. H. & Hart, S. R. (1986). Chemical geodynamics. *Annual Review of Earth and Planetary Sciences* **14**, 493–571.